HHS Public Access

Author manuscript

Nat Immunol. Author manuscript; available in PMC 2023 November 03.

Published in final edited form as:

Nat Immunol. 2023 April ; 24(4): 652–663. doi:10.1038/s41590-023-01441-0.

I-A^{g7} β56/57 polymorphisms regulate non-cognate negative selection to CD4 T cell orchestrators of type-1 diabetes

Brian D. Stadinski[1], **Sarah B. Cleveland**[1], **Michael A. Brehm**[2], **Dale L. Greiner**[2], **Priya G. Huseby**[1], **Eric S. Huseby**[1,*]

[1]Department of Pathology, University of Massachusetts Medical School, Worcester, MA 01655, USA

[2]Department of Molecular Medicine, Diabetes Center of Excellence, University of Massachusetts Medical School, Worcester, MA 01655, USA

Summary:

Genetic susceptibility to type-1 diabetes is associated with homozygous expression of MHC-II alleles that that carry specific β-chain polymorphisms. Why heterozygous expression of these MHC-II alleles does not confer a similar predisposition remains unresolved. Using a NOD mouse model, we demonstrate that heterozygous expression the T1D protective allele, I-A^{g7} β56P/57D, induces significant negative selection to the I-A^{g7}-restricted T cell repertoire, including β-islet specific CD4 T cells. Surprisingly, negative selection occurs despite I-A^{g7} β56P/57D having a significantly reduced ability to present β-islet antigens to CD4 T cells. Peripheral manifestations of non-cognate negative selection include a near complete loss of β-islet specific CXCR6^{+} CD4 T cells, an inability to cross-prime IGRP and Insulin specific CD8 T cells and disease arrest at the insulitis stage. These data reveal that negative selection on non-cognate self-antigens in the thymus can promote T cell tolerance and protection from autoimmunity.

Introduction:

Type-1 diabetes (T1D) results from an autoimmune-mediated destruction of the islets of Langerhans β cells within the pancreas, leaving the body with an inability to produce insulin [1, 2, 3]. The autoimmune disease process is thought to be stepwise and progressive, due to the requirement of hurdling multiple checkpoints to carry out β-cell destruction. The non-obese diabetic (NOD) mouse serves as the primary animal model for T1D, developing lymphocytic infiltrations into islet cell masses prior to the onset of hyperglycemia. The exact events precipitating a pathogenic response are not fully understood but are thought to

*Correspondence: Eric.Huseby@umassmed.edu, Phone: (508) 856-2180, Fax: (508) 856-1094.

AUTHOR CONTRIBUTIONS

B.D.S. and E.S.H. conceived and designed the project and interpreted experiments; B.D.S. performed TCR cloning and sequencing, flow cytometry, adoptive T cell transfer experiments, monitored disease and statistical analyses; S.B.C. performed histological analyses and T cell activation studies; M.A.B. and D.L.G. provided PBMC from HLA typed individuals with and without T1D; P.G.H. generated specific mouse lines and monitored disease; B.D.S. and E.S.H. wrote the manuscript.

Competing interests

The authors declare no competing interests

involve multiple cell types including CD4 and CD8 T cells, B lymphocytes, macrophages and dendritic cells [4, 5, 6, 7].

Susceptibility to developing T1D is heritable and polygenic, with approximately half of the genetic risk mapping to the major histocompatibility locus (MHC) [8]. The association primarily results from the expression of specific DQB1 alleles, in particular the homozygous expression of DQB1*02:01 (DQ2.5), DQB1*03:02 (DQ8), or their heterozygous combination [9]. These HLA-DQB1 alleles, as well as the NOD mouse I-A^{g7} allele, uniquely carry non-Asp residues within the MHC P9 pocket at position 57 [10, 11, 12, 13]. It is postulated that these MHC-II polymorphisms limit the diversity of self-peptides, including islet-associated self-peptides, presented to developing thymocytes but not within peripheral tissues where antigen concentrations can be higher [14, 15, 16, 17]. Particular MHC-II alleles may also allow unusual peptide sequences to be presented or normally ignorant self-reactive T cells to be primed by molecular mimics [18, 19]. Confounding a simple functional interpretation for the role of MHC alleles in T1D susceptibility are observations that expression of a single copy of DQ2.5 or DQ8, as well as NOD mice expressing I-A^{g7} in combination with a second MHC allele, largely abrogates increased susceptibility to T1D development [10, 20, 21, 22, 23, 24, 25].

How heterozygous expression of MHC-II alleles influences autoimmune susceptibility remains unresolved [26]. MHC-II heterozygosity expands the immunopeptidome, relative to homozygosity, based on each MHC-II's peptide binding characteristics. Manifestation of this 'expansion of self' will occur during T cell development and mature T cell homeostasis. During thymic selection, increased peptide diversity may promote negative selection or the development of tissue-specific regulatory T cells if the co-expressed MHC-II allele has enhanced ability to present cognate autoantigens. In the periphery, MHC-II heterozygosity may limit or alter the activation and differentiation of autoimmune T cells, due to a halving of the presentation of autoantigens, or via regulatory T cells restricted to the 'protective' MHC-II allele [26, 27, 28, 29]. To address these and other possible mechanisms, we analyzed the autoimmune cascade in MHC-II heterozygous NOD mice that express one allele of I-A^{g7} and one allele of I-A^{g7} carrying the 'protective' MHC-IIβ 56P/57D polymorphisms (I-$A^{g7\text{-}PD}$).

We present evidence that heterozygous expression of I-$A^{g7\text{-}PD}$ induces thymic negative selection of self-reactive I-A^{g7}-restricted CD4 T cells that normally develop in NOD mice. This culling includes β-islet specific CD4 T cells and occurs during the first wave of thymic negative selection, thereby precluding the diversion of these clones into the $Foxp3^+$ T_{reg} lineage [30]. Intriguingly, negative selection occurs despite I-$A^{g7\text{-}PD}$ having a significantly reduced ability to present β islet-antigens to I-A^{g7}-restricted clones, nor is I-$A^{g7\text{-}PD}$ capable of presenting allo-peptides that activates β-islet specific T cells. Thus, negative selection is occurring on non-cognate self-pMHC distinct from the periphery targeted autoantigens. Manifestation of this non-cognate negative selection include a limited ability of the remaining β islet-specific CD4 T cells to differentiate into the $CXCR6^+$ lineage, and an inability to induce cross-priming of IGRP- and Insulin-specific CD8 T cells. $CXCR6^+$ CD4 T cells are shown to be sufficient to elicit cross-priming of β-islet CD8 T cells and drive the T1D disease process. Thus, our findings demonstrate that negative selection on non-cognate

self-pMHC can promote immune tolerance in part by the removal of CD4 T cells that orchestrate β-islet specific CD8 T cell priming and targeting of pancreatic islets.

Results:

I-A$^{g7\text{-}PD}$ heterozygosity prevents targeting of pancreatic islets by CD8 T cells

To study the role of MHC-II polymorphisms in T1D susceptibility, we generated NOD mice expressing I-A^{g7} β56P/57D (I-A$^{g7\text{-}PD}$) and I-A^{g7}-deficient (I-A$^{g7\text{-}KO}$) mice using CRISPR/Cas9 techniques (Extended Data Fig. 1a,b and methods). Individual founder lines were bred with our colony of NOD mice for six generations, and then intercrossed to generate two cohorts with the resultant MHC-II genotypes: I-Ag7-WT/WT, I-Ag7-PD/WT and I-Ag7-PD/PD, and I-Ag7-WT/WT, I-Ag7-KO/WT and I-A$^{g7\text{-}KO/KO}$. Co-housed female mice were monitored for the development of diabetes for 50 weeks. NOD I-A$^{g7\text{-}WT/WT}$ mice developed T1D at a frequency of ~80%, with no differences in frequency observed in mice derived from I-A$^{g7\text{-}PD/WT}$ or I-A$^{g7\text{-}KO/WT}$ intercross breeding (Fig. 1a and Extended Data Fig. 1c,d).

NOD mice heterozygous (I-A$^{g7\text{-}PD/WT}$) or homozygous (I-A$^{g7\text{-}PD/PD}$) for the I-A$^{g7\text{-}PD}$ allele are resistant to disease. For I-A$^{g7\text{-}PD/WT}$ mice, diabetes developed in ~3% (2/61) of the mice examined. Disease resistance in I-A$^{g7\text{-}PD/WT}$ mice did not result from decreased expression of the wild type I-A^{g7} MHC allele; NOD mice carrying only a single copy of I-A^{g7} (I-A$^{g7\text{-}KO/WT}$) are highly susceptible to T1D (~60%) despite expressing approximately half the amount of MHC-II, whereas I-A$^{g7\text{-}KO/KO}$ mice remained disease free (Fig. 1a, Extended Data Fig. 1b–h). Consistent with disease susceptibility, pancreatic islets of 12 weeks old I-A$^{g7\text{-}WT/WT}$ and IA$^{g7\text{-}WT/KO}$ mice were heavily infiltrated with lymphocytes, whereas I-A$^{g7\text{-}PD/WT}$ mice displayed predominately peri-insulitic lesions (Extended Data Fig. 1i–k).

Striking differences in the activated/memory T cell infiltrate were observed between T1D susceptible and resistant strains. These included a ~5-fold increase in the number of activated CD8 T cells, and a modest increase in activated CD4 T_{conv} cells, in I-A$^{g7\text{-}WT/WT}$ and I-A$^{g7\text{-}KO/WT}$ mice as compared to I-A$^{g7\text{-}PD/WT}$ mice (Fig. 1b, c). As previously noted [31], the majority of activated islet-infiltrating CD4 T_{conv} cells were CD44^{hi} VLA4^{+} CXCR6^{+} FR4^{lo} (CXCR6^{+} CD4 T cells, [32]), or CD44^{hi} VLA4^{+} FR4^{+} CXCR6^{neg} (FR4^{+} CD4 T cells, [33]). In I-A$^{g7\text{-}PD/WT}$ mice, however, there was a selective ~3.5-fold loss of the CXCR6^{+} CD4 T cells, relative to I-A$^{g7\text{-}WT/WT}$ mice, while the frequency of FR4^{+} CD4 T cells was unchanged (Fig. 1d–f). Further analyses demonstrated a reduction in β-islet specific Chromogranin A hybrid insulin peptide ($ChgA_{HIP}$)- and islet amyloid polypeptide hybrid insulin peptide ($IAPP_{HIP}$)-specific CD4 T cells, and a near complete absence of glucose-6-phosphatase, catalytic, 2 ($IGRP_{206–214}$) and $Insulin_{15–23}$ reactive CD8 T cells infiltrating the pancreas of I-A$^{g7\text{-}PD/WT}$ mice (Fig. 1g–n). Thus, T1D susceptibility and the targeting of β-islets by CD4 and CD8 T cells can be regulated by heterozygous expression of I-A^{g7} β56P/57D polymorphisms.

I-A^{g7} β56/57 polymorphisms control self-reactive CD4 T cell development

The T1D disease resistance of I-A$^{g7\text{-}PD/WT}$ mice suggest that heterozygous expression of the I-A$^{g7\text{-}PD}$ allele alters the development and/or function of pathogenic I-A^{g7}-restricted CD4 T cell clones. To address developmental aspects of this hypothesis, we first analyzed thymocyte subsets in female 6-weeks old mice. Robust generation of CD4SP thymocytes occurred in I-A$^{g7\text{-}WT/WT}$ and I-A$^{g7\text{-}KO/WT}$ mice, whereas CD4SP are reduced ~25% in thymocytes isolated from I-A$^{g7\text{-}PD/WT}$ and I-A$^{g7\text{-}PD/PD}$ mice. The CD4SP reduction largely accounts for the modest reduction in overall thymic cellularity observed between I-A$^{g7\text{-}PD}$ expressing as compared to non-expressing mice. No changes were observed in the CD4^{-}CD8^{-} or CD8SP compartment, the frequency within the CD4SP compartment at which Foxp3^{+} thymic T$_{regs}$ are generated or overall TCR Vβ gene usage (Fig. 2a–d and Extended Data Fig. 2a–f).

Alterations in T cell development between I-A$^{g7\text{-}WT/WT}$ and I-A$^{g7\text{-}PD/WT}$ mice first manifest at the CD4^{+}CD8^{+} (DP) stage. The frequency at which DP thymocytes undergo the initial stages of positive selection, the DP CD69^{lo} to DP CD69^{hi} transition was similar in each of the I-A^{g7} β56/57 congenic mice. However, I-A$^{g7\text{-}PD}$-expressing mice showed ~25% reduction in thymocyte subset frequencies, relative to I-A$^{g7\text{-}WT/WT}$ mice, starting at the TCRβ^{int} to TCRβ^{hi} transition, a developmental stage where negative selection can occur, which continued through differentiation of mature CD4SP (Fig. 2e–i and Extended Data Fig. 2b). Consistent with the hypothesis of increased frequencies of negative selection, I-A$^{g7\text{-}PD}$-expressing dendritic cells (DCs) were ~30% more capable of activating pre-selection DP thymocyte, as compared to I-A^{g7}-expressing DCs (Extended Data Fig. 2f–k). The higher frequency at which DP thymocytes are eliminated in mice expressing I-A$^{g7\text{-}PD}$, however, did not translate into mature CD4 T cell isolated from I-A$^{g7\text{-}WT/WT}$ mice having high frequencies of alloreactivity; splenic CD4 T$_{conv}$ cells isolated from I-A$^{g7\text{-}WT/WT}$ mice responded to I-A$^{g7\text{-}PD}$, as well as I-A^{b}, expressing DCs at a frequency of ~3% (Fig. 2j–l). This frequency of alloreactivity was similar to CD4 T$_{conv}$ isolated from I-A$^{g7\text{-}PD/PD}$ as well as C57BL/6 mice and represents an ~10-fold decrease in frequency at which the expression of I-A$^{g7\text{-}PD}$ limited the generation of CD4SP. These data argue that co-expression of the I-A$^{g7\text{-}PD}$ allele eliminates a large fraction of I-A^{g7}-restricted thymocytes via TCR-self-pMHC interactions that are below the stimulatory threshold of mature T cell proliferation.

We sought to define characteristics of CD4 T cells that develop in NOD mice with or without the co-expression of I-A$^{g7\text{-}PD}$. We have reported that T cell repertoires biased towards self-reactivity carry increased frequencies of hydrophobic amino acids within the combining sites of CDR3β segments [34]. Using this metric, CD4 T$_{conv}$ cells isolated from I-A$^{g7\text{-}WT/WT}$ and I-A$^{g7\text{-}KO/WT}$ mice showed a strong increase in the usage of hydrophobic residues, relative to NOD.*H-2A^{b}* mice that express I-A^{b}, a non-disease promoting MHC-II allele (Fig. 3a). In contrast, no differences were observed for CD4 T$_{conv}$ cells isolated from I-A$^{g7\text{-}PD/WT}$ and I-A$^{g7\text{-}PD/PD}$ mice or in CD8 T cells isolated from each of the strains (Fig. 3b). Similarly, CD4 T cells, but not CD8 T cells, isolated from individuals with T1D carrying predisposing haplotypes demonstrated an enrichment in CDR3β hydrophobic residues, relative to non-T1D individuals (Fig. 3c,d and Extended Data Fig. 3).

A TCR clonotype analyses was next performed to reveal the extent for which expression of the I-$A^{g7\text{-}WT}$ and I-$A^{g7\text{-}PD}$ alleles modulate the CD4 T cell repertoire that develops in I-$A^{g7\text{-}PD/WT}$ mice. The 500 most frequent $Va2^+$ CD4 and CD8 T cell clonotypes that develop in I-$A^{g7\text{-}WT/WT}$ and I-$A^{g7\text{-}PD/PD}$ mice that express a transgenic TCRβ chain were defined, and the frequency at which they occur in I-$A^{g7\text{-}PD/WT}$ mice was determined. Morisita-Horn analyses revealed contributions of both I-A^{g7}- and I-$A^{g7\text{-}PD}$-restricted CD4 T cell clonotypes in I-$A^{g7\text{-}PD/WT}$ mice. However, the contribution of each T cell repertoire was not equivalent, with the CD4 T cell repertoires in I-$A^{g7\text{-}PD/WT}$ mice being more similar to that of I-$A^{g7\text{-}PD/PD}$ mice, as compared to I-$A^{g7\text{-}WT/WT}$ mice (Fig. 3e). In contrast, because the MHC-I allele are identical in the mice being studied, CD8 T repertoire biases were not observed (Fig. 3f). Because extensive CD4 T cell clonal overlap in I-$A^{g7\text{-}WT/WT}$ and I-$A^{g7\text{-}PD/PD}$ mice was detected, we examined the fate of T cells uniquely restricted to I-A^{g7} or I-$A^{g7\text{-}PD}$, based on a >10-fold selection bias (Fig. 3g). For these clonotypes, we observed a ~2.5-fold increased frequency at which I-$A^{g7\text{-}PD}$ eliminated I-A^{g7}-restricted clones, relative to I-A^{g7} eliminating I-$A^{g7\text{-}PD}$-restricted clones (Fig. 3h). Shared T cell clones, <10-fold selection bias, were equally represented in I-$A^{g7\text{-}PD/WT}$ mice (Fig. 3i). Interestingly, the I-$A^{g7\text{-}WT}$-restricted T cell clones that are reduced >10-fold due to I-$A^{g7\text{-}PD}$ expression were not found to be enriched in the $Foxp3^+$ T_{reg} lineage (Fig. 3j,k), an observation consistent with I-$A^{g7\text{-}PD}$ expression inducing negative selection at the DP stage of thymocyte development. Collectively, these data argue that non-cognate negative selection on self-peptide/I-$A^{g7\text{-}PD}$ complexes eliminates many of the self-reactive CD4 T cells normally carried in the NOD T cell repertoire.

Co-expression of I-$A^{g7\text{-}PD}$ purges islet-specific CD4 T cells by non-cognate negative selection

To reveal the influences heterozygous expression of I-$A^{g7\text{-}PD}$ has on β-islet specific CD4 T cell development, $ChgA_{HIP}$- and $IAPP_{HIP}$-specific CD4SP thymocytes were analyzed using a tetramer-based pulldown approach. $ChgA_{HIP}$ and $IAPP_{HIP}$ are the cognate β-islet antigens recognized by the high affinity autoimmune CD4 T cell clones, BDC2.5 and BDC6.9 [35, 36, 37]. In I-$A^{g7\text{-}WT/WT}$ mice, I-A^{g7}-$ChgA_{HIP}$ and I-A^{g7}-$IAPP_{HIP}$ $tetramer^{bright}$ and $tetramer^{dim}$ CD4SP populations were observed. However, in I-$A^{g7\text{-}PD/WT}$ mice, the pMHC $tetramer^{bright}$ CD4SP populations were largely absent, whereas the number of pMHC $tetramer^{dim}$ CD4SP were unchanged (Fig. 4a–h). Consistent with these findings, BDC2.5 TCR Tg mice demonstrated a ~3-fold decrease in mature CD4SP thymocytes when bred onto a I-$A^{g7\text{-}PD/WT}$ or I-$A^{g7\text{-}PD/PD}$ genetic background (Extended Data Fig. 4a–d). Similar to altered CD4 T cell development in polyclonal mice (Fig. 3), reduced thymocyte development in I-$A^{g7\text{-}PD}$ expressing BDC2.5 TCR Tg mice was first observable at the DP $CD69^+$ $TCR\beta^{hi}$ stage (Extended Data Fig. 4e–h).

To formally test whether positive or negative selection pressures limit the development of high affinity β-islet specific T cells in I-$A^{g7\text{-}PD}$ expressing mice, irradiated I-$A^{g7\text{-}WT/WT}$, I-$A^{g7\text{-}PD/WT}$, I-$A^{g7\text{-}PD/PD}$ and I-A^b expressing C57BL/6 mice were reconstituted with bone marrow (BM) from I-$A^{g7\text{-}WT/WT}$ mice. In these BM chimeric mice, negative selection mediated by BM-derived APCs is limited to the I-$A^{g7\text{-}WT}$ allele whereas positive selection can occur on the MHC-II alleles expressed on cortical thymic epithelial cells (cTECs) within

the host mice. Analyses of $ChgA_{HIP}$-specific T cell development revealed that I-$A^{g7\text{-}PD/WT}$ mice reconstituted with I-$A^{g7\text{-}WT/WT}$ BM generated similar numbers of pMHC tetramer^{bright} CD4 T cells as compared to I-$A^{g7\text{-}WT/WT}$ host mice (Extended Data Fig 5a–d). To further assess whether to the I-$A^{g7\text{-}WT}$ allele is functional on TECs in I-$A^{g7\text{-}PD/WT}$ mice, cortical and medullary TECs were isolated from I-$A^{g7\text{-}WT/WT}$, I-$A^{g7\text{-}PD/WT}$ and I-$A^{g7\text{-}PD/PD}$ mice and used as APC to activate $ChgA_{HIP}$-specific T cells. cTECs and mTECs isolated from I-$A^{g7\text{-}WT/WT}$ and I-$A^{g7\text{-}PD/WT}$ mice, but not I-$A^{g7\text{-}PD/PD}$ mice, were similarly capable of activating $ChgA_{HIP}$-specific T cells (Extended Data Fig. 5e–h). These data argue that the I-$A^{g7\text{-}WT}$ allele is functionally expressed on cTECs in I-$A^{g7\text{-}PD/WT}$ mice, and that BM-derived thymic APCs expressing I-$A^{g7\text{-}PD}$ are capable of targeting high affinity $ChgA_{HIP}$-specific thymocytes for negative selection.

We next probed whether negative selection of $ChgA_{HIP}$ and $IAPP_{HIP}$ reactive thymocytes in I-$A^{g7\text{-}PD/WT}$ mice might arise from cognate or non-cognate recognition of self-pMHC ligands. Interestingly, APCs exclusively expressing I-$A^{g7\text{-}PD}$ had an ~100-fold reduced ability to activate $ChgA_{HIP}$-reactive T cells to soluble peptide or β islet cell antigens (Fig. 4i,j and Extended Data Fig. 4i–l), and have a near complete inability to present $IAPP_{HIP}$ to T cells (Fig. 4k,l). Consistent with this observation, the I-$A^{g7\text{-}PD}$ allele was observed to be ~25 and 100-fold less capable of binding the $ChgA_{HIP}$ and $IAPP_{HIP}$ peptides, respectively (Fig. 4m–o). In addition, I-$A^{g7\text{-}PD}$ did not present an allogeneic self-peptide ligand to BDC2.5 or BDC6.9 T cells capable of inducing activation. Consistent with these *in vitro* studies, adoptively transferred BDC2.5 TCR Tg CD4 T cells underwent proliferation in recipient mice that express the I-$A^{g7\text{-}WT}$ allele, but not in I-$A^{g7\text{-}PD/PD}$ recipient mice (Fig. 4p,q). These data argue that β-islet specific thymocytes can be subject to negative selection following recognition of self-peptide/I-$A^{g7\text{-}PD}$ ligands that are distinct from the cognate autoantigen targeted within the pancreas and below the stimulatory potency required for mature CD4 T cell activation.

I-$A^{g7\text{-}PD/WT}$ mice carry reduced frequencies of β-islet specific CXCR6$^+$ CD4 T cells

Manifestations of non-cognate negative selection on I-$A^{g7\text{-}PD}$ include altering the differentiation patterns of β-islet specific CD4 T cells. In I-$A^{g7\text{-}WT/WT}$, I-$A^{g7\text{-}KO/WT}$ and I-$A^{g7\text{-}PD/WT}$, $ChgA_{HIP}$- and $IAPP_{HIP}$-reactive CD4 T cells were found expanded and mostly displayed an activated, CD44^{hi} VLA4$^+$ phenotype, as compared to CD4 T cells in I-$A^{g7\text{-}PD/PD}$ mice (Fig. 5a,b and Extended Data Fig. 6 a,b). Within these β-islet specific populations, differentiation of CXCR6$^+$ CD4 T cells was largely exclusive to I-$A^{g7\text{-}WT/WT}$ and I-$A^{g7\text{-}KO/WT}$ mice and occurred coincident with the ability to be stained brightly with $ChgA_{HIP}$ and $IAPP_{HIP}$ pMHC tetramers (Fig. 5c–j). In contrast, similar numbers of β-islet specific FR4$^+$ CD4 T cells were present in all mice expressing at least one copy of the I-$A^{g7\text{-}WT}$ allele, and $ChgA_{HIP}$- and $IAPP_{HIP}$-specific Foxp3$^+$ T_{regs} represent minute populations in all mice (Extended Data Fig. 6c–j).

The correlation between tetramer staining and differentiation into CXCR6$^+$ CD4 T cells suggested that the strength of TCR signals might contribute to this differentiation process. To evaluate this hypothesis, we first isolated $ChgA_{HIP}$-specific CD4 T cells from I-$A^{g7\text{-}WT/WT}$ and I-$A^{g7\text{-}PD/WT}$, converted these cells into hybridomas, stained the resultant

clones with $ChgA_{HIP}$ tetramers and identified the antigen potency, as readout as EC_{50} value of IL-2 production (Fig. 5k–n). I-A^{g7}-$ChgA_{HIP}$ tetramer^{bright} T cells isolated from I-$A^{g7\text{-}WT/WT}$ mice were found ~100-fold more reactive to $ChgA_{HIP}$ as compared to $ChgA_{HIP}$ tetramer^{dim} T cells isolated from I-$A^{g7\text{-}PD/WT}$ mice (Fig. 5n). In addition, this diverse set T cell clonotypes was significantly less well activated by APCs exclusively expressing I-$A^{g7\text{-}PD}$, regardless of mouse source or potency (Extended Data Fig 6k–o). As expected, the ability to be stained with pMHC tetramers correlated with the antigen potency of the T cell (Fig. 5o), supporting the hypothesis that I-$A^{g7\text{-}WT/WT}$ mice carry a population of high affinity β-islet specific CD4 T cells that are eliminated in I-$A^{g7\text{-}PD/WT}$ mice.

To further evaluate the contribution of TCR-pMHC affinity in the acquisition of CD4 T cell effector mechanisms, we employed the B3k506 TCR Tg model paired with a panel of peptide ligands with equilibrium affinities that range from strong to weak affinity (K_D 7–278μM) [38]. Naïve B3k506 TCR transgenic T cells were stimulated with titrating concentration of each peptide ligand and a clear hierarchy of response is observed; proliferation and expression of FR4 and VLA4, an integrin required for T cells to traffic into tissues [39], required the weakest TCR signal strength, based on equilibrium affinity (K_D) and antigen concentration (Fig. 5p). CXCR6 expression required an additional 1–2 $\log_{10}$ greater antigen concentration or an ~3-fold increase in ligand affinity. Expression of CD40L, a molecule critical for the maturation and licensing of dendritic cell and CD8 T cell help [40, 41, 42, 43], required the strongest TCR signals. Indeed, for CD40L expression, only the ligand with K_D of 7μM was capable of inducing its maximal expression at 1μM antigen concentration (Fig. 5q and Extended Data Fig. 6p). These data support the hypothesis that non-cognate negative selection in I-$A^{g7\text{-}PD/WT}$ mice includes the targeting of high affinity β-islet specific clones capable of differentiating into $CXCR6^+$ CD4 T cells.

$CXCR6^+$ CD4 T cells orchestrate β-islet specific CD8 T cell activation and T1D

The coincident loss of $CXCR6^+$ CD4 T cells and CD8 T cells targeting the pancreas in I-$A^{g7\text{-}PD/WT}$ mice suggests interplay between these subsets influence T1D susceptibility. To monitor the fate of β-islet specific CD8 T cells, we stained peripheral CD8 T cells with H2-K^d tetramers carrying $IGRP_{206–214}$ or $Insulin_{15–23}$ epitopes [44, 45]. For both β-islet specificities, CD8 T cells were 10–25-fold expanded and displayed an activated/memory phenotype in I-$A^{g7\text{-}WT/WT}$ mice, as compared to I-$A^{g7\text{-}PD/WT}$ mice (Fig. 6a–d). These differences are likely a product of altered CD8 T cell priming; infection with recombinant VSV carrying β-islet antigens induced robust IGRP- and Insulin-specific CD8 T cell responses in both I-$A^{g7\text{-}WT/WT}$ and I-$A^{g7\text{-}PD/WT}$ mice, indicating CD8 T cells with these specificities are present in I-$A^{g7\text{-}PD/WT}$ mice (Extended Data Fig. 7a–d). In addition, adoptive transfer of $IGRP_{206–214}$-specific NY8.3 TCR Tg CD8 T cells (NY8.3 CD8 T cells) into NOD I-$A^{g7\text{-}WT/WT}$ and I-$A^{g7\text{-}KO/WT}$ recipient mice showed robust proliferation, whereas NY8.3 CD8 T cells remained undivided when transferred into I-$A^{g7\text{-}PD/WT}$ and I-$A^{g7\text{-}PD/PD}$ hosts, as well as mice deficient in ab T cells (TCR $Ca^{-/-}$) or MHC-II molecules (I-$A^{g7\text{-}KO/KO}$) (Fig. 6e,f). These data indicate that particular CD4 T cells, which are absent in I-$A^{g7\text{-}PD}$-expressing mice, are required to elicit MHC-I cross-priming of CD8 T cells to these islet-antigen.

Functionally, polyclonal and islet-specific CXCR6^{+} but not FR4^{+} CD4 T cells upregulated CD40L expression following activation (Fig. 7a–d and Extended Data Fig. 7e,f), and when transferred into recipient mice, induced MHC-I cross-priming of IGRP specific T cells (Fig. 7e,f). In addition, co-transfer of CXCR6^{+} but not FR4^{+} CD4 T cells with polyclonal CD8 T cells into NOD TCR Ca$^{-/-}$ recipient mice rapidly induced T1D. Disease was not observed in recipient mice that received CXCR6^{+} CD4 T cells or polyclonal CD8 T cells independently (Fig. 7g,h). Thus, CXCR6^{+} and FR4^{+} CD4 T cells have different abilities to elicit β-islet specific CD8 T cell activation and T1D progression.

Discussion

T cell-mediated autoimmune diseases occur when a breakdown of tolerance mechanisms allows lymphocytes to target healthy cells within tissues. The role of MHC-II alleles in promoting and limiting susceptibility has been studied for many years, but there remain unresolved questions: To what extent are defects in self-tolerance imprinted during thymic selection versus a product of dysregulated T cell homeostasis? Are tolerance defects repertoire-wide or limited to a handful of inflammatory or regulatory T cell clones? How does heterozygous expression of a ‘protective’ MHC-II alleles influence the development and function of pathogenic CD4 and CD8 T cell clones? The data we have presented here offer some insight into these questions.

We compared T cell development in NOD mice that exclusively express I-A^{g7} to ones that co-express the T1D ‘protective’ allele I-A$^{g7\text{-}PD}$. In conventional NOD mice, self-reactive CD4 T cells undergo positive selection and orchestrate T1D. However, when one allele of I-A$^{g7\text{-}PD}$ is expressed, negative selection is significantly enhanced at the DP stage of T cell development. This culling includes β-islet specific tetramer^{bright} thymocytes and allows only a self-reactive T cell repertoire with limited autoimmune potential to develop in I-A$^{g7\text{-}PD/WT}$ mice. Remarkably, thymic elimination of pathogenic CD4 T cells does not follow the standard model of negative selection; I-A$^{g7\text{-}PD}$ does not present either ChgA$_{HIP}$ or IAPP$_{HIP}$ efficiently to T cells. Thus, autoimmune T cells can be targeted for negative selection following recognition of non-cognate self-pMHC within the thymus.

TCRs have an inherent ability to recognize multiple distinct peptides presented by MHC molecules. This cross-reactivity is highlighted by the ability of T cells to undergo positive selection and peripheral homeostasis on ‘non-cognate’ self-pMHC, while simultaneously being capable of rapid clonal expansion following recognition of pathogen-derived pMHC molecules [46, 47]. TCR cross-reactivity also occurs to peptides bound to different MHC alleles, termed alloreactivity. Alloreactivity carried within mature T cell repertoires is thought to occur at a rate of ~1–3% per MHC haplotype [48], a rate we similarly observe for mature CD4 T cells isolated from I-A$^{g7\text{-}WT/WT}$ as well as I-A$^{g7\text{-}PD/PD}$ mice. Recognition of self-peptide/I-A$^{g7\text{-}PD}$ ligands by DP thymocytes in NOD mice, however, limits T cell selection by ~25%, an ~10-fold greater rate than alloreactivity. The implication of these findings is that the hyper-sensitivity of DP thymocytes to TCR stimuli [49, 50, 51, 52], allows self-pMHC interactions that are below the stimulatory potency required for mature CD4 T cell activation to nevertheless induce negative selection [53]. Although the self-pMHC ligands that induce non-cognate negative selection are currently unknown, discrepancies between

the frequency at which negative selection occurs in I-$A^{g7\text{-}WT/WT}$ and I-$A^{g7\text{-}PD/WT}$ mice may result from the I-A^{g7} MHC molecules having a limited capacity to present a diverse array of peptides [37, 54], thereby limiting the number of self-pMHC species that can act as non-cognate negative selecting ligands.

Non-cognate negative selection and its manifestations on β-islet specific CD4 T cell repertoires are highlighted by the behavior of $ChgA_{HIP}$- and $IAPP_{HIP}$-reactive thymocyte and mature T cell. $ChgA_{HIP}$- and $IAPP_{HIP}$-reactive thymocytes are subject to negative selection in I-$A^{g7\text{-}PD}$-expressing mice despite I-$A^{g7\text{-}PD}$ having an ~100-fold decrease in ability to present the autoantigen. *In vitro* and *in vivo* studies further demonstrate that I-$A^{g7\text{-}PD}$ does not present an allo-peptide capable of activating mature BDC2.5 CD4 T cells. The process of non-cognate negative selection on I-$A^{g7\text{-}PD}$ ligands, however, does not generate enhanced frequencies of $ChgA_{HIP}$- or $IAPP_{HIP}$-specific $Foxp3^+$ T_{regs}. This thymic deletion without $Foxp3^+$ T_{reg} diversion phenotype likely results from the thymocyte developmental stage at which self-antigen recognition first occurs. Negative selection occurs at two stages during T cell development, at the DP stage within the thymic cortex, and as immature CD4SP or CD8SP thymocytes migrate through the thymic medulla [55, 56]. The predominant branch of CD4 $Foxp3^+$ T_{reg} development occurs co-incident with the ‘second wave’ of negative selection [57]. Thus, our observation that non-cognate negative selection initiates at the DP stage, likely mediated by cortical dendritic cells, may preclude the opportunity of these clones to later audition for $Foxp3^+$ T_{reg} selection [30].

Within the mature T cell repertoire, β-islet specific CD4 T cells in I-$A^{g7\text{-}WT/WT}$ mice can acquire a $CXCR6^+$ phenotype, whereas the $ChgA_{HIP}$- and $IAPP_{HIP}$-reactive T cells that escape non-cognate negative selection in I-$A^{g7\text{-}PD/WT}$ mice demonstrate a paucity of these cells. Studies further suggest the strength of TCR signals derived from self-pMHC recognition contributes to these patterns of CD4 T cell differentiation; acquisition of the $CXCR6^+$ phenotype appears coincident with CD4 T cells staining brightly with the $ChgA_{HIP}$ and $IAPP_{HIP}$ tetramers and presumably receiving an IL-12 cytokine signal [32]. Further, naïve CD4 T cells require higher affinity or concentrations of antigen to induce CXCR6 expression as compared to proliferation or FR4 or VLA4 expression. How activated CD4 T cells that initially express both FR4 and CXCR6 ultimately differentiate into each lineage(s) remains unknown. However, the hierarchal acquisition of effector functions likely explains why $CXCR6^+$ CD4 T cells, but not $FR4^+$ CD4 T cells, are selectively decreased within the lymphocytic infiltrate of the pancreas of T1D resistant I-$A^{g7\text{-}PD/WT}$ mice as compared to T1D susceptible I-$A^{g7\text{-}WT/WT}$ mice.

The ability of non-cognate negative selection to limit the development of $tetramer^{bright}$/high affinity β-islet specific CD4 T cells capable of acquiring a $CXCR6^+$ phenotype likely has important autoimmune disease susceptibility consequences. In NOD mice, MHC-I molecules cross-present β-islet antigens to CD8 T cells [58, 59, 60, 61, 62]. However, coincident with the severe reduction of β-islet specific $CXCR6^+$ CD4 T cells in I-$A^{g7\text{-}PD/WT}$ mice, spontaneous CD8 T cell priming to IGRP and Insulin does not occur. MHC-I cross-priming of IGRP also does not occur in MHC-II- or T cell-deficient mice as well, suggesting that MHC-I cross-presentation of β-islet antigens to naïve CD8 T cells is induced by specific CD4 T cells and not suppressed in I-$A^{g7\text{-}PD/WT}$ mice via regulatory mechanisms. Indeed,

CXCR6^{+} but not FR4^{+} CD4 T cells are capable of upregulating CD40L following T cell activation, an effector function that requires very strong TCR signals to induce and is required for DC licensing [40, 41, 42, 43, 63]. Importantly, complementation studies reveal that MHC-I cross-priming of IGRP-reactive CD8 T cells is inducible by NOD derived CXCR6^{+} CD4 T cells, and in the presence of CD8 T cells, leads to T1D. These observations are consistent with studies demonstrating that both CD4 and CD8 T cell subsets are required for T1D [7], and argue that β-islet specific CXCR6^{+} CD4 T cells regulate CD8 T cell functional responses and susceptibility to T1D. Thus, one manifestation of non-cognate negative selection is to eliminate CD4 T cells capable of licensing DC to cross-present β-islet antigens on MHC-I molecules and orchestrate T1D.

Methods

Mice:

NOD-Foxp3-gfp (NOD/ShiLt-Tg(Foxp3-EGFP/cre)1cJbs/J) mice, NY8.3 TCR tg mice (NOD.Cg-Tg(TcraTCRbNY8.3)1Pesa/DvsJ), BDC2.5 TCRtg (NOD.Cg-Tg(TcraBDC2.5,TCRbBDC2.5)Doi/DoiJ), and NOD.β2m$^{-/-}$ (NOD.129P2(B6)-*B2m*^{tm1Unc}/J) were purchased from The Jackson Laboratory (Bar Harbor, ME). NOD.Ca$^{-/-}$ mice were a kindly provided by Dr Roland Tisch (University of North Carolina, Chapel Hill NC). NOD YAeB62 Tg mice were generated in house by breeding of the C57Bl/6.YAe62β Tg line to NOD.Foxp3-gfp for 10 generations. TCRα$^{+/-}$ TCRβ$^{+/-}$ MHCI/II deficient Nr4a1-GFP (Nur77-GFP) mice were generated in house as previously described [34]. Bone marrow chimeric mice were generated as previously described [64], and analyzed at 6 weeks post transfer.

NOD.I-A$^{g7PD/PD}$ mice were made at the UMASS Mutagenesis Core Facility by co-injection hCas9 and gRNA (TCATGATGTTATTCGTCATG) and single-stranded donor oligonucleotide (TGCGCTTCGACAGCGACGTGGGCGAGTACCGCGCGGTGACCGAGCTGGGGCGCCCCGACGCAGAGTACTACAATAAGCAGTACCTGGAGCGAACGCGGGCCGAGCTGGACAC) into NOD zygotes isolated from super pregnant NOD females purchased from Taconic Farms (Germantown, NY). The resulting pups were screened for alterations in I-A^{g7} locus by sequencing PCR amplicons; KOD polymerase kit (Sigma Millipore) with the following primers (GGGGGGGAATTCCATTTCGTGCACCAGTTCAAG) (CCCCCCGAATTCCAGCCCTCACAAGACAAGCGT) (ThermoFisher). This approach introduced only two amino acid changes in the coding region of I-A^{g7} within the NOD mouse genome, ensuring that all of the other T1D susceptibility loci are intact, and that the mutant MHC-II is under the same regulatory control as the wild type I-A^{g7} allele. Simultaneously, we generated NOD mice deficient in I-A^{g7} expression due to a frame shift mutation in the I-A^{g7} β chain coding sequence (I-A$^{g7\text{-}KO/KO}$) (Figure S1). Founder mice were backcrossed to NOD-Foxp3-gfp mice for 6 generations followed by intercrossing of the line. All mouse sub-lines were maintained in a pathogen-free environment in accordance with institutional guidelines in the Animal Care Facility at the University of Massachusetts Medical School.

Antibodies:

Antibodies against mouse antigens included: anti-TCRβ (H57–597), anti-CD25 (PC61), anti-CXCR6 (SA051D1), anti-VLA4 (R1–2), anti-FR4 (12A5) anti-CD19 (6D5), anti-I-A^{g7} (OX6), anti-CD11c (N418), anti-K^{d} (SF1–1.1), anti-XCR1 (ZET), anti-CD4 (RM4–5), anti-CD69 (H1.2F3) Biolegend; anti-CD4 (GK1.5), anti-CD4, anti-Vβ8 (F23.1), anti-Vβ4 (KT4), anti-Thy1–2 (53–2.1), anti-CD44 (IM7), anti-CD69 (H1.2F3) BD Biosciences anti-CD8 (5H10), anti-B220 (RA3–6B2) ThermoFisher. Antibodies against human antigens included: anti-CD4 (SK3), anti-CD45RO (UCHL1), anti-CCR7 (G043H7) Biolegend and anti-CD8 (RPA-T8), anti-CD127 (HI-L7R-M21), anti-CD19 (HIB19), anti-CD27 (L128), anti-CD3 (SK7), anti-CD25 (M-A251), anti-CD95 (DX2) BD Biosciences. All antibody staining was conducted with 1:300 dilutions unless otherwise stated.

IDDM development:

Cohorts of female NOD.I-$A^{g7WT/WT}$, NOD.I-$A^{g7KO/WT}$, NOD.I-$A^{g7PD/WT}$, NOD.I-$A^{g7PD/PD}$, NOD.I-$A^{g7KO/KO}$ mice were monitored weekly for urine glucose beginning at 5 weeks of age until 50 weeks of age for the development of T1D. Mice were considered to have developed IDDM when urine glucose was >500mg/dL (Diastix, Bayer) on 2 consecutive tests followed by a blood glucose reading >250mg/dL (Freestyle lite, Abbott Labs).

Histology.

The pancreases of NOD. I-$A^{g7WT/WT}$, NOD. I-$A^{g7KO/WT}$, NOD. I-$A^{g7PD/WT}$, NOD. I-$A^{g7PD/PD}$ 12 weeks of age were fixed in 10% formalin embedded in paraffin and sectioned and. 8 sections 400μm apart from each pancreas and stained with hematoxylin and eosin. Islets were scored for lymphocytic infiltrates, utilizing a scoring system with 4 grades: 1 no infiltration, 2 peri-insulitis, 3 < 50% of islet infiltrated, 4 > 50% of islets infiltrated.

Tetramer production.

Recombinant I-A^{g7} molecules were produced in insect cells as in [35]. Peptides were encoded at the N terminus of the I-A^{g7} beta chain followed by a gly-ser linker; ChgA-HIP peptide (LQTLALWSRMD) and IAPP-HIP (LQTLALNAARDP) [36]. Recombinant K^{d} molecules were produced in insect cells along with peptides linked to β2m using baculovirus. K^{d} molecules contain a point mutation Y48A at the carboxy terminus of the binding groove to accommodate a gly-ser linker. Peptides were encoded at the N terminus of β2m followed by a GGGSGG linker; IGRP (VYLKTNVFL) and the Insulin(I9) (LYLVCGERI) variant for improved K^{d} binding [65]. Monomeric I-A^{g7} molecules and K^{d} molecules were biotinylated with recombinant BirA (Avidity, Aurora CO) and mixed at 1:8 or 1:6 molar ratios, respectively, with streptavidin-PE (PJRS25–1) (Agilent, Santa Clara CA).

Cell surface staining and tetramer enrichment.

Single cell suspension of splenocytes and pancreases from mice 12–16 weeks of age were prepared by mechanical disruption, lysed with hypotonic Gey's solution and stained with the following antibodies: anti-TCRβ, anti-CD25, anti-CXCR6, anti-VLA4, anti-FR4, anti-CD4, anti-CD44, anti-CD8, anti-B220. B cells and DCs from mice 4–6 weeks of age were

stained with the following antibodies: anti-TCRβ, anti-CD19, anti-CD11c, anti-I-A^{g7}, anti-K^d, anti-XCR1. B cells were defined as (TCRβ^{neg}, CD19$^+$), DCs were defined as (TCRβ^{neg}, CD19^{neg} cells, CD11c$^+$, I-A^{g7+}, XCR1$^+$ or XCR1^{neg}). Thymocytes from mice 4–6 weeks of age were stained with the following antibodies: anti-TCRβ (1:200), anti-CD4 (1:150), anti-CD69, anti-K^d, anti-CD25, anti-CD8 (1:150), anti-B220. All antibodies were used at a 1:300 dilution unless otherwise stated. All mice analyzed expressed the foxp3-GFP transgene. Tetramer staining was carried out in the presence of 50nM dasatinib (Sigma), cells were incubated with dasatinib for 30min at 37c, then incubated for 1hrs with 10μg/mL MHCII tetramer or MHCI tetramer coupled to PE at 22c. Tetramer-stained cells were subsequently enriched using anti-PE microbeads (Miltenyi) following established protocols. Analysis of flow cytometric data was performed using FlowJo version 9.9.6 (TreeStar).

Generation and Activation of T cell hybridomas.

$ChgA_{HIP}$ tetramer positive CD4 T cells were flow sorted from I-$A^{g7\ WT/WT}$ and I-$A^{g7\ PD/WT}$ mice, stimulated for 5 days on plate bound αCD3 and αCD28 in RPMI media supplemented with 10U IL-2 and and converted into hybridomas as previously described [66]. For activation studies, 10^6 splenocytes from I-$A^{g7\ WT/WT}$, I-$A^{g7\ PD/WT}$, I-$A^{g7\ PD/PD}$ NOD mice were co-cultured with 10^5 BDC2.5 or BDC 10.1 T hybridomas plus soluble $ChgA_{HIP}$ (LQTLALWSRMD) peptide (AALabs, San Diego CA) or islet cell perpetrations [35], and incubated for 24hrs at 37c. The concentration of IL-2 in these cultures was determined through serial dilution of the supernatant and subsequent culture with the IL-2 dependent cell line HT-2 for 24hrs [30].

Thymocyte pre-selection activation assay.

Activation of DP thymocytes was carried out a previously described [34]. Briefly, thymocytes isolated from TCRα$^{+/-}$ TCRβ$^{+/-}$ MHCI/II deficient mice expressing Nur77-GFP. 5 × 10^6 thymocytes were co-cultured with 3 × 10^5 BMDCs for 16 h in 2 ml D-MEM with 10 μM Z-VAD-FMK (ENZO) in a 24 well plate. Z-VAD was used to keep the thymocytes from undergoing apoptosis during the culture period. BMDCs were generated from β2m$^{-/-}$ I-$A^{g7\text{-}WT/WT}$, I-$A^{g7\text{-}PD/PD}$, I-$A^{g7\text{-}KO/KO}$ NOD mice and β2m$^{+/+}$ I-$A^{g7\ WT/WT}$, I-$^{Ag7\ PD/PD}$ NOD mice, as well as NOD.H2b mice. Following co-culture, cells were surface stained for 30min at 22c with anti-TCRβ, anti-B220, anti-CD4, anti-CD8 and anti-CD69. Thymocytes were gated for expression of TCRβ, CD4$^+$, CD8$^+$, B220^{neg} and analyzed for the upregulation of CD69 and Nur77-GFP.

Assay of peptide binding to I-A^{g7} and I-$A^{g7\text{-}PD}$.

Soluble I-A^{g7} and I-$A^{g7\text{-}PD}$ with covalently attached pHEL were treated with thrombin to cleave the linker attaching the peptide to the I-A^{g7} β chain [35]. Samples (0.5 μg) were incubated with a soluble biotinylated version of pHEL, Biotin-GGGMKRHGLDNYRGYSL, (11 μM), either alone or in the presence of various concentrations of competitor peptides in 15 μl of pH 5.5 buffer overnight at 21°C. The samples were diluted to 100 μl of PBS in a well of a 96-well ELISA plate coated with an I-A^{g7} monoclonal antibody, OX6 (BD Pharmaceuticals). The captured I-A^{g7} and I-$A^{g7\text{-}PD}$ were washed several times with PBS and the bound bio-pHEL detected with akaline phosphatase coupled Extravadin (Sigma) and *o*-nitrophenol phosphate.

Human Subjects.

21 individuals (11 with T1D, 10 without T1D) were provided informed consent and recruited into this study under the approval of the Institutional Review Board at the University of Massachusetts School of Medicine, Worcester MA.

Sorting mouse and human T cells.

3 independent sets of mouse splenic CD4 T_{conv} and CD8 T cells from I-$A^{g7\ WT/WT}$, I-$A^{g7\ KO/WT}$, I-$A^{g7\ PD/WT}$, and I-$A^{g7\ PD/PD}$ NOD mice were magnetically enriched with either CD4 or CD8 microbeads (Miltenyi), stained with anti-TCRβ, anti-B220, anti-CD4, anti-CD8, anti-CD62L and CD44 and sorted for naïve CD4 T cells (TCRβ^{+}, B220^{neg}, CD4^{+}, foxp3-gfp^{neg}, CD62L^{+}, and CD44^{low}) or naïve CD8 T cells (TCRβ^{+}, B220^{neg}, CD8^{+}, CD62L^{+}, and CD44^{low}) BD FACS Aria. Human PBMCs were isolated from blood samples obtained by venipuncture using sodium heparin as anticoagulant following Ficoll-Paque (GE Healthcare) separation and stained with the following antibodies prior to sorting (BD FACS Aria): anti-CD4, anti-CD45RO, anti-CCR7, anti-CD8, anti-CD127, anti-CD19, anti-CD27, anti-CD3, anti-CD25, anti-CD95, for naïve CD4 T_{conv} (CD3^{+}, CD19^{neg}, CD4^{+}, CD25^{neg}, CD127^{low}, CD27^{+}, CD45RO^{neg}, CCR7^{+}, CD95^{neg}) and naïve CD8 T cells (CD3^{+}, CD19^{neg}, CD8^{+}, CD27^{+}, CD45RO^{neg}, CCR7^{+}, CD95^{neg}).

TCR cDNA library construction and sequencing.

Creation of TCRβ and TCRα libraries were carried out as previously described [30, 34] Briefly, sorted T cells were re-suspended in 1 ml Tryzol (Life Technologies), and RNA was extract according to the manufacturer's protocol using 20ug/mL RNase free glycogen (Life Technologies) as a carrier. cDNA was generated from up to 2 μg of RNA by priming with 10 μM oligo(dT) (Promega) and was extended with Omniscript RT kit (Qiagen) following the manufacturer's protocol. PCR amplification of murine and human TCRs were done using a two-step, nested primer approach. First, 20-cycle PCR reactions were used to amplify the TCR Vβ or TCR Vα genes using the appropriate PCR primers. The mouse Vβ primer sequences were as follows:

Vβ2, GGGGCATATGGAGGCTTTGCTGGAGCAAAACCCAAGGTGG;

Vβ6, GGAACCAAACATATGGAGGCTATCATTACTCAGACACCC;

Vβ8.2, ATCCTCGAGAGGAATGGACAAGATCCTGACAGC;

TCR Cβ, CTTGGGTGGAGTCACATTTCTCAGATCCTC.

The human Vβ primer sequences were as follows:

TRBV10–3, CTTGGGTGGAGTCACATTTCTCAGATCCTC;

TRBV19, CAGTCCCCAAAGTACCTGTTCAGA;

TRVB28, GATGTGAAAGTAACCCAGAGCTCG;

TRBC, ACTGTGCACCTCCTTCCCATTCAC.

The mouse TCR Vα primer sequences were as follows: Vα2 primer

(5′-CCCTGGGGAAGGCCCTGCTCTCCTGATA-3′) and TCR Cα primer (5′-GGTACACAGCAGGTTCTGGGTTCTGGATG-3′).

1/10th of the primary reaction was used as the template for a second 20-cycle PCR reaction to add on the adaptor sequences and barcodes to identify samples post-sequencing. TCRβ sequencing was performed on an Illumina HiSeq 2000, 100bp single read, while TCRα sequencing was performed on an Illumina MiSeq, 250bp single read, at the University of Massachusetts Deep Sequencing Core Facility.

Processing TCRβ sequence data.

Individual T cell subsets from 3 sets of mice per MHC haplotype were analyzed independently and used as biological replicates. Primary sequence reads were first filtered to remove low quality reads (Q score <25). Sequence data sets were parsed by the sample bar code using the program fastq-multx (52). TCR Vβ and Jβ gene segments or in the case of TCRβ tg mice Vα and Jα gene segments were identified, and CDR3 base-pair sequence reads were converted to amino acid sequence using the program TCRKlass [67]. CDR3β sequences were aligned by sequence, with the conserved Cys with the Vβ gene segment labeled position 1, and the conserved FG amino acids in Jβ gene segments as the last two positions of the CDR3β. The aligned reads were then stratified into different groups, based on TCR Vβ chain identity and the length of the CDR3β sequence (12–16-mer). Within each of these groups, the occurrence of each of 400 possible CDR3β amino acid doublets at P6 and P7 was counted, and a 400-by-1 vector of doublet counts was generated for each sample replicate. Thus, 400-by-1 vectors summarized the census of CDR3β P6-P7 doublets within each replicate library and each sample. Counts were normalized to frequencies, and average frequencies were calculated for each Vβ in each sample (mouse Vβ2, 6, 8; human TRBV10–3, 19, 28), Doublet motifs with an average frequency greater than 5×10^{-5} among the samples and a probability of enrichment <0.05, unpaired two-tailed t-test were compared and the sum of doublets enriched in each sample was determined. The summation was stratified based on whether a doublet can promote, is neutral or limits self-reactivity [34] and the probability mass function, p, calculated using a hypergeometric test (Excel) is displayed on each graph.

TCRα count matrixes from the TCRβ Tg populations, CD4 T_{conv} (n=4) and CD4 T_{reg} (n=3), were rank ordered based on abundance. The counts of the top 1000 clonotypes from each sample were determined across all samples and used to calculate the Morisita-Horn index, EstimateS ver9.1.0 to estimate the relative overlap of clonotypes between samples. TCR clonotypes with greater than 10-fold enrichment between TCRβ Tg I-$A^{g7\text{-}WT/WT}$ and I-$A^{g7\text{-}PD/PD}$ or I-$A^{g7\text{-}WT/WT}$ and I-$A^{g7\text{-}PD/WT}$ T_{conv} populations were determined using DESeq2 [68] in R (v4.0.0) utilizing TMM normalization. The counts of the top 1000 clonotypes with greater than and less than 10-fold enrichment from each sample were determined across all samples and used to calculate the Morisita-Horn index (EstimateS).

In vitro activation/differentiation of CD4 T cells.

10^6 spenocytes from 506TCR.Rag$^{-/-}$ mice were co cultured with BMDCs from C57BL/6 mice along with 3-fold dilutions and cognate 3K peptide (FEAQKAKANKAVD) as well as previously defined altered peptide ligands P-1A (FEAAKAKANKAVD), P8A (FEAQKAKANAAVD) or P2A (FEAQKAAANKAVD). Upregulation of CD40L was determined after 6hrs following co-culture; VLA-4, FR4 and proliferation were assessed on day 2, while CXCR6 was determined on day 7 following the addition of IL-12 (20ng/mL) between days 1–5 [32]. The maximum level of marker expression was determined from cell stimulation with cognate 3K peptide at 10μg/mL. Relative stimulation levels were calculated following background subtraction from wells containing T cells and DCs alone. CD40L upregulation on CXCR6$^+$ and FR4$^+$ subsets were determined on splenocytes magnetically enriched using CD4 microbeads (Miltenyi) from NOD mice 8 weeks of age at 4hrs following stimulation with plate bound anti-CD3 (2C11, 1μg/mL) and anti-CD28 (3F12, 4μg/mL) (BioXcel). 10^6 spenocytes from BDC2.5TCR mice were co cultured with 1×10^5 BMDCs and titrating numbers of islet cells. Frequency of CD4$^+$ CD44$^+$ CTV^{dim} cells was determined following 3 days co-culture. Isolation of TECs were done following the published protocol in reference [69].

In vivo proliferation of β-islet specific CD4 and CD8 T cells.

8×10^6 splenocytes from NY8.3 TCR transgenic mice or BDC2.5 TCR transgenic mice were labeled with cell trace violet (CTV) (ThermoFisher) according to the manufactures protocol and i.v. transferred into 8 weeks old recipient mice. Pancreatic and inguinal LNs from recipient mice were harvested 3 days post-transfer and analyzed by flow cytometry following staining with the following antibodies: anti-TCRβ, anti-B220, anti-CD4, anti-CD8, anti-CD44 Biolegend, anti-Vβ8, anti-Vβ4 BD Biosciences. Transferred cells were gated for expression of TCRβ, CTV, CD4 and Vβ4 (BDC2.5) or CD8 and Vβ8 (NY8.3).

CXCR6 and FR4 cell transfers.

Splenocytes from non-diabetic NOD females 14–16 weeks of age were sequentially magnetically enriched using CD4 then CD8 microbeads (Mitenyi). The CD4 enriched fraction was subsequently stained with anti-Thy1–2, anti-CD44, anti-CD4, anti-CXCR6, anti-FR4 and sorted for CXCR6$^+$ CD4 T cells (Thy1–2$^+$, CD4$^+$, Foxp3-GFP^{neg}, CD44$^+$, FR4^{low} CXCR6$^+$) or FR4$^+$ CD4 T cells (Thy1–2$^+$, CD4$^+$, Foxp3-GFP^{neg}, CD44$^+$, FR4$^+$ CXCR6^{neg}). 1.2×10^6 sorted CXCR6$^+$ or FR4$^+$ CD4 T cell populations or 1.5×10^6 CD8 T cells were transferred i.v. into recipient NOD.Ca$^{-/-}$ mice as indicated. Recipient mice were monitored for the development of IDDM for 16 weeks post transfer.

Statistical analysis.

Experimental results were analyzed for significance using one-way analysis of variance (ANOVA) with Tukey's multiple comparisons test or unpaired two-tailed *t*-test, Specific tests to evaluate significance are included in the figure captions. Statistical analyses were performed using Prism version 7.04 (GraphPad software). $P < 0.05$ was considered significant (* $P < 0.05$; ** $P < 0.01$; *** $P < 0.001$; **** $P \leq 0.0001$). Hypergeometric distributions were calculated in Excel.

Data availability:

TCR sequencing data is available through the NIH SRA:SRR16314909, SRR16314908, SRR16314907, SRR16314905, SRR16314906, SRR16314942, SRR16314941, SRR16314940, SRR16314939, SRR16314938, SRR16314937, SRR16314936, SRR16314935, SRR16314934, SRR16314933, SRR16314932, SRR16314931, SRR16314926, SRR16314925, SRR16314924, SRR16314930, SRR16314929, SRR16314928, SRR16314927, SRR16314923, SRR16314946, SRR16314945, SRR16314944, SRR16314943, SRR16314921, SRR16314920, SRR16314919, SRR16314918, SRR16314917, SRR16314916, SRR16314915, SRR16314922, SRR16314914, SRR16314913, SRR16314912, SRR16314911, SRR16314910, SRR16313009, SRR16313011, SRR16313010, SRR16313008, SRR16313013, SRR16313012, SRR16313057, SRR16313056, SRR16313062, SRR16313061, SRR16313060, SRR16313059, SRR16313058

Extended Data

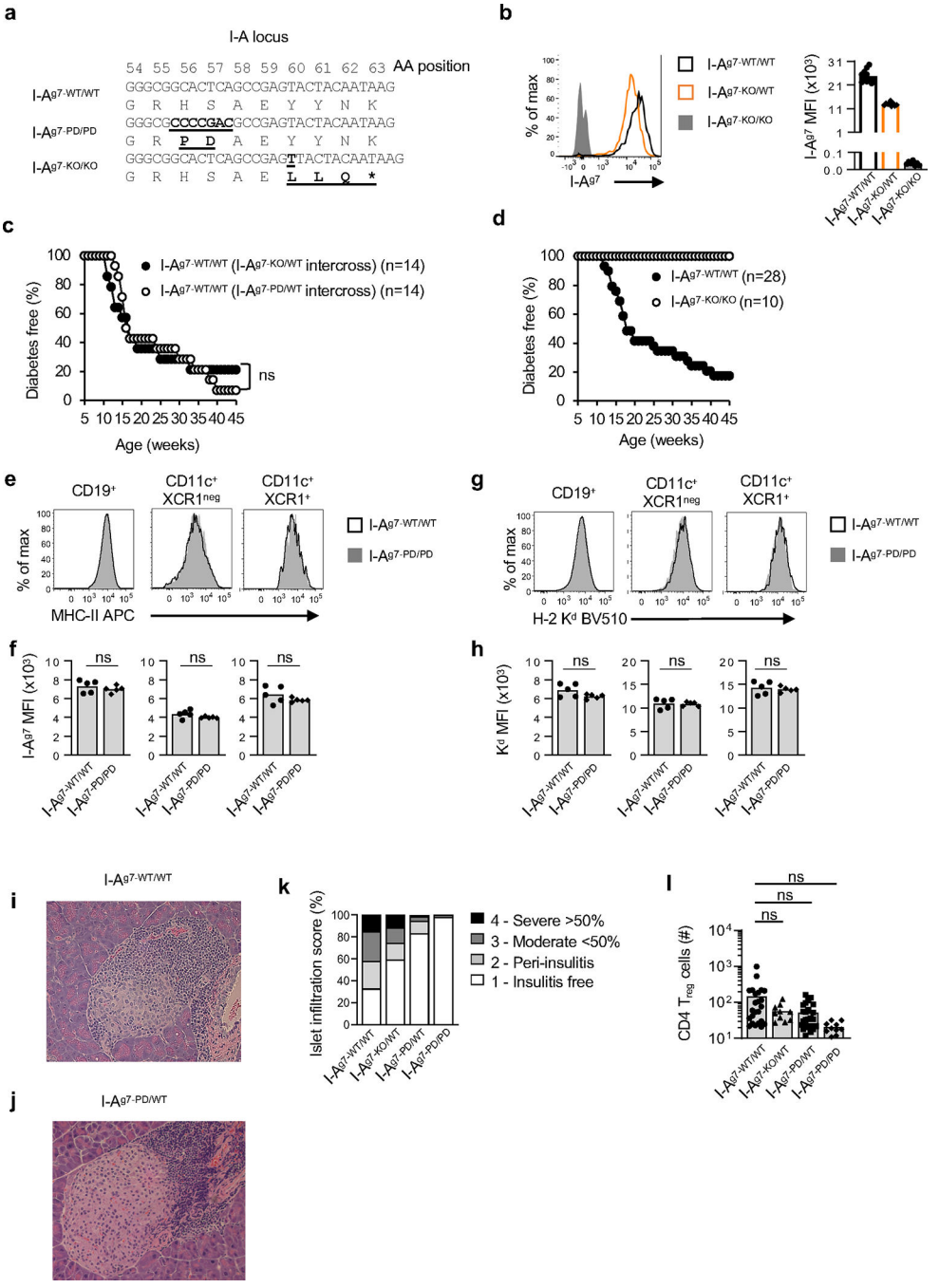

Extended Data Fig. 1. Characterization of NOD mice carrying different combinations of I-A^{g7} β56/57 polymorphisms.

(**a**) Genomic DNA sequence surrounding I-A^{g7} β56/57 of NOD mice carrying the wild type (HS), PD or frame shift (KO) mutation. (**b**) MHC-II expression on B cells from I-A$^{g7\text{-}WT/WT}$ and I-A$^{g7\text{-}KO/KO}$ mice. (**c**) T1D incidence in I-A$^{g7\text{-}WT/WT}$ mice derived from intercrossing I-A$^{g7\text{-}PD/WT}$ or I-A$^{g7\text{-}KO/WT}$ mice. ns P>0.05, logrank Mantel-Cox test. (**d**) T1D incidence in I-A$^{g7\text{-}KO/KO}$ and I-A$^{g7\text{-}WT/WT}$ mice derived from intercrossing I-A$^{g7\text{-}KO/WT}$ mice. (**e-h**)

Cell surface expression of MHC molecules on APC subsets. (**e, f**) I-A^{g7} and (**g, h**) H2-K^{d} expression level and average mean fluorescence intensity (MFI) of $CD19^{+}$ B cells, $CD11c^{+}$ $XCR1^{neg}$ cDC2 and $CD11c^{+}$ $XCR1^{pos}$ cDC1 from I-$A^{g7\text{-}WT/WT}$ (n=5) and I-$A^{g7\text{-}PD/PD}$ (n=5) mice. (**i,j**) Representative hematoxylin and eosin staining of a grade 3 islet and grade 1 islet from the pancreas from I-$A^{g7\ WT/WT}$ and I-$A^{g7\ PD/WT}$ bearing mice, respectively. (**k**) Average frequency of islet infiltration severity at 12 weeks of age (n=8) using a four scale grade: 0 - insulitis free, 1- peri-insulitis, 2 – moderate <50% infiltrated, 3 – severe >50% infiltration. (**l**) Quantification of $Foxp3^{+}$ regulatory T cell subsets within the pancreatic infiltrate of NOD mice carrying different combinations of I-A^{g7} β56/57 polymorphisms. ns $P>0.05$; * $P<0.05$; ** $P<0.01$ (one-way ANOVA with Tukeys multiple comparisons test).

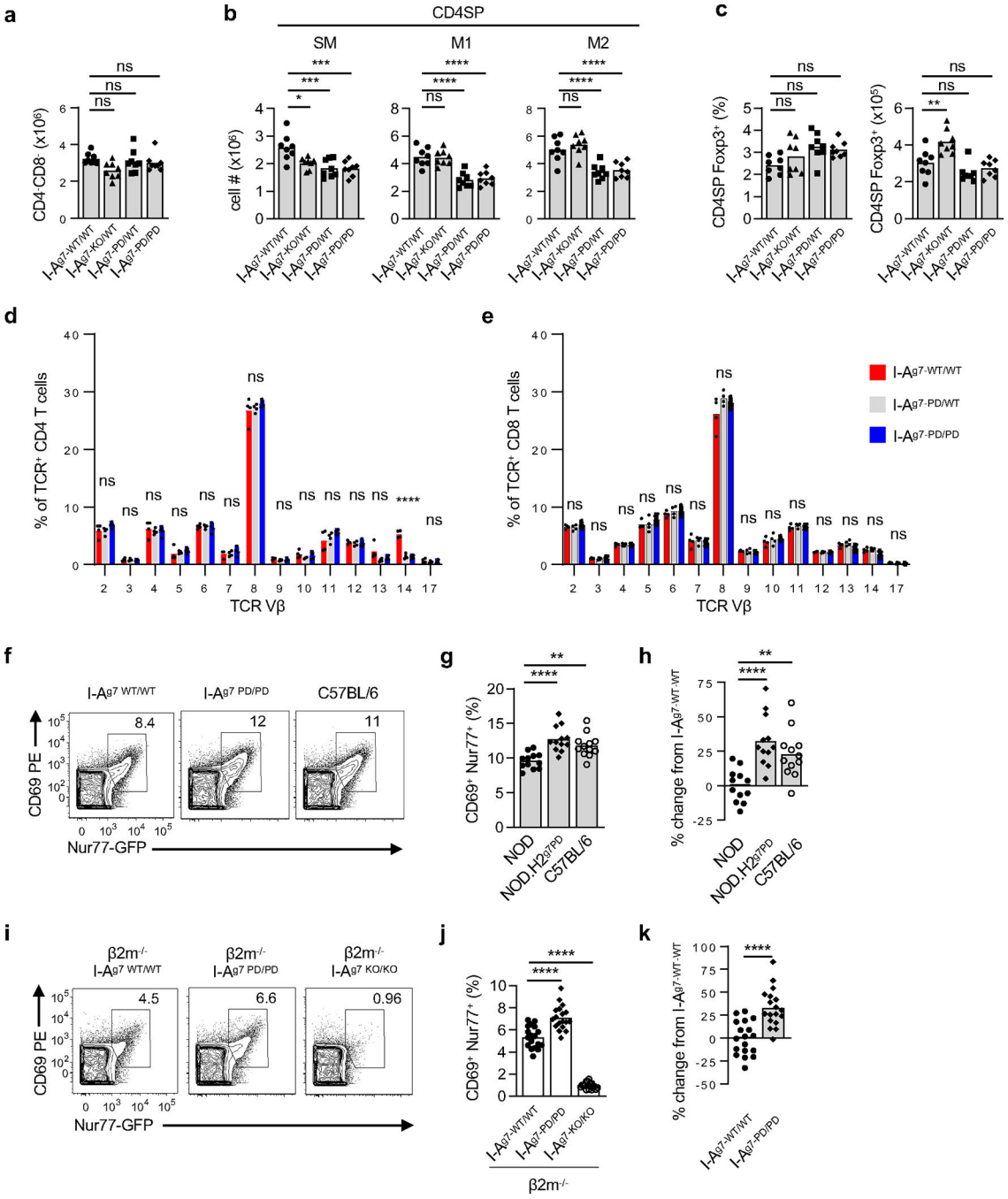

Extended Data Fig. 2.

Characterization of thymic T cell selection in 6 weeks old I-A$^{g7\text{-}WT/WT}$, I-A$^{g7\text{-}KO/WT}$, I-A$^{g7\text{-}PD/WT}$ and I-A$^{g7\text{-}PD/PD}$ mice (n=8). (**a**) Total number of CD4^{-}CD8^{-} and (**b**) semimature (SM), mature 1 (M1) and mature 2 (M2) CD4SP thymocyte generated in each strain. (**c**) Percent of CD4SP and total number of Foxp3+ CD4SP thymocytes generated in each strain. (**d-e**) Frequencies of TCR Vβ^{+} T cells among (d) CD4^{+} and (e) CD8^{+} subsets in I-A$^{g7\text{-}WT/WT}$, I-A$^{g7\text{-}PD/WT}$ and I-A$^{g7\text{-}PD/PD}$ mice. (**f**) Representative dot plots of CD69 and Nur77-GFP expression on pre-selection TCRβ^{+} DP thymocytes derived from 4–6 weeks old

Nur77-gfp^{+} *H2-Ab1*$^{-/-}$ *B2m*$^{-/-}$ (MHC-deficient) mice following co-culture with BM-DCs generated from I-A$^{g7\text{-}WT/WT}$, I-A$^{g7\text{-}PD/PD}$ or C57BL/6 (H-2^{b}) mice. (**g**) Quantification of the frequency and (**h**) percent of H-2^{g7} reactivity at which DP thymocytes from 6 mice express CD69 and Nur77-GFP following culture with BM-DC from 2 independent mice. Data are from 2 independent experiments. (**i**) Representative dot plots of CD69 and Nur77-GFP expression on pre-selection TCRβ^{+} DP thymocytes (n=6) derived from 4–6 weeks old Nur77-gfp^{+} *H2-Ab1*$^{-/-}$ *B2m*$^{-/-}$ (MHC-deficient) mice following co-culture with BM-DCs generated from 3 β2M$^{-/-}$ I-A$^{g7\text{-}WT/WT}$, β2M$^{-/-}$ I-A$^{g7\text{-}PD/PD}$ or β2M$^{-/-}$ I-A$^{g7\text{-}KO/KO}$ mice. (**j**) Quantification of the frequency and (**k**) percent of I-A^{g7} reactivity at which DP thymocytes express CD69 and Nur77-GFP following culture with BM-DC. Data are from 2 independent experiments. ns P>0.05; * P<0.05; ** P<0.01; *** P<0.001; **** P<0.0001 (one-way ANOVA with Tukeys multiple comparisons test).

a

Sample #	Disease Status	A2	DR3	DR4	Assigned Serological Interpretation	Sample #	Disease Status	A2	DR3	DR4	Assigned Serological Interpretation
1	Healthy	+			DQ7 DQ5	12	T1D	+	+	+	DQ2 DQ8
2	Healthy	+			DQ6 DQ6	13	T1D		+	+	DQ2 DQ8
3	healthy	+			DQ7 DQ4	14	T1D		+		DQ2 DQ2
4	healthy				DQ7 DQ6	15	T1D		+	+	DQ2 DQ8
5	healthy				DQ5 DQ6	16	T1D		+		DQ2 DQ2
6	healthy				DQ9 DQ5	17	T1D	+	+	+	DQ2 DQ8
7	healthy				DQ4 DQ6	18	T1D	+	+	+	DQ2 DQ8
8	healthy				DQ5 DQ6	19	T1D		+	+	DQ2 DQ8
9	healthy	+			DQ7 DQ3	20	T1D		+		DQ2 DQ2
10	healthy	+			DQ9 DQ6	21	T1D			+	DQ8 DQ8
11	healthy				DQ9 DQ6						

b

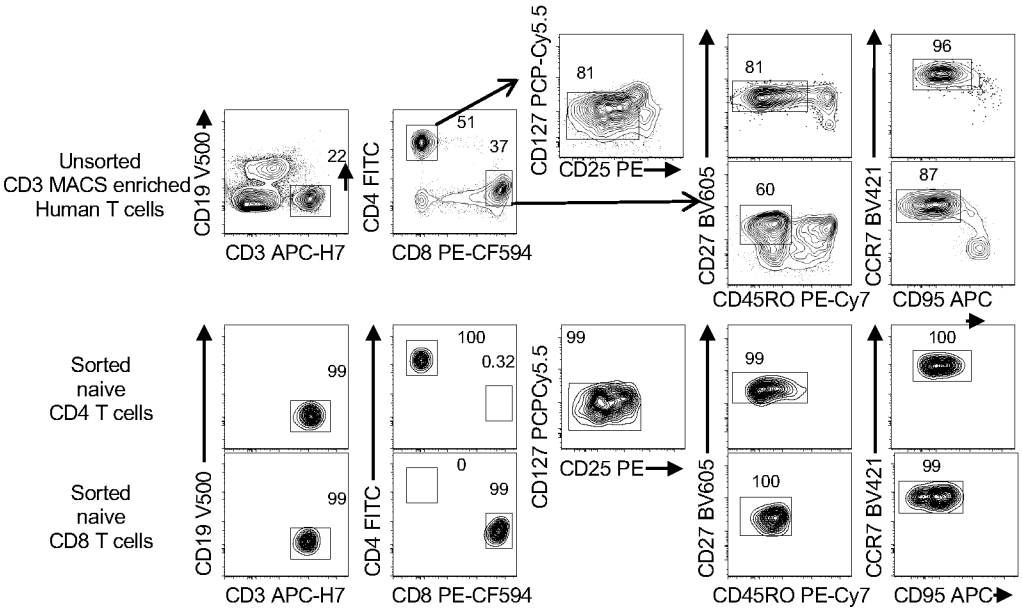

Extended Data Fig. 3. HLA analyses and representative flow cytometry sorting of donors with T1D and healthy controls and Morisita-Horn analysis of T cell repertoires.

(**a**) HLA status of donors, including positivity or negativity for HLA-A2, HLA-DR3, HLA-DR4, and HLA-DQ usage. (**b**) Example of flow cytometry sorting of human samples for isolation of naïve CD4 and naïve CD8 T cells. All TCR^+ lymphocytes were sorted based on being a single cell that expresses CD3 and CD4 or CD8. CD4 T_{conv} cells were further sorted for the expression of CD25 and CD127, and CD27, CD45RO, CCR7 and CD95. CD8 T_{conv} were further sorted for the expression of CD27, CD45RO, CCR7 and CD95.

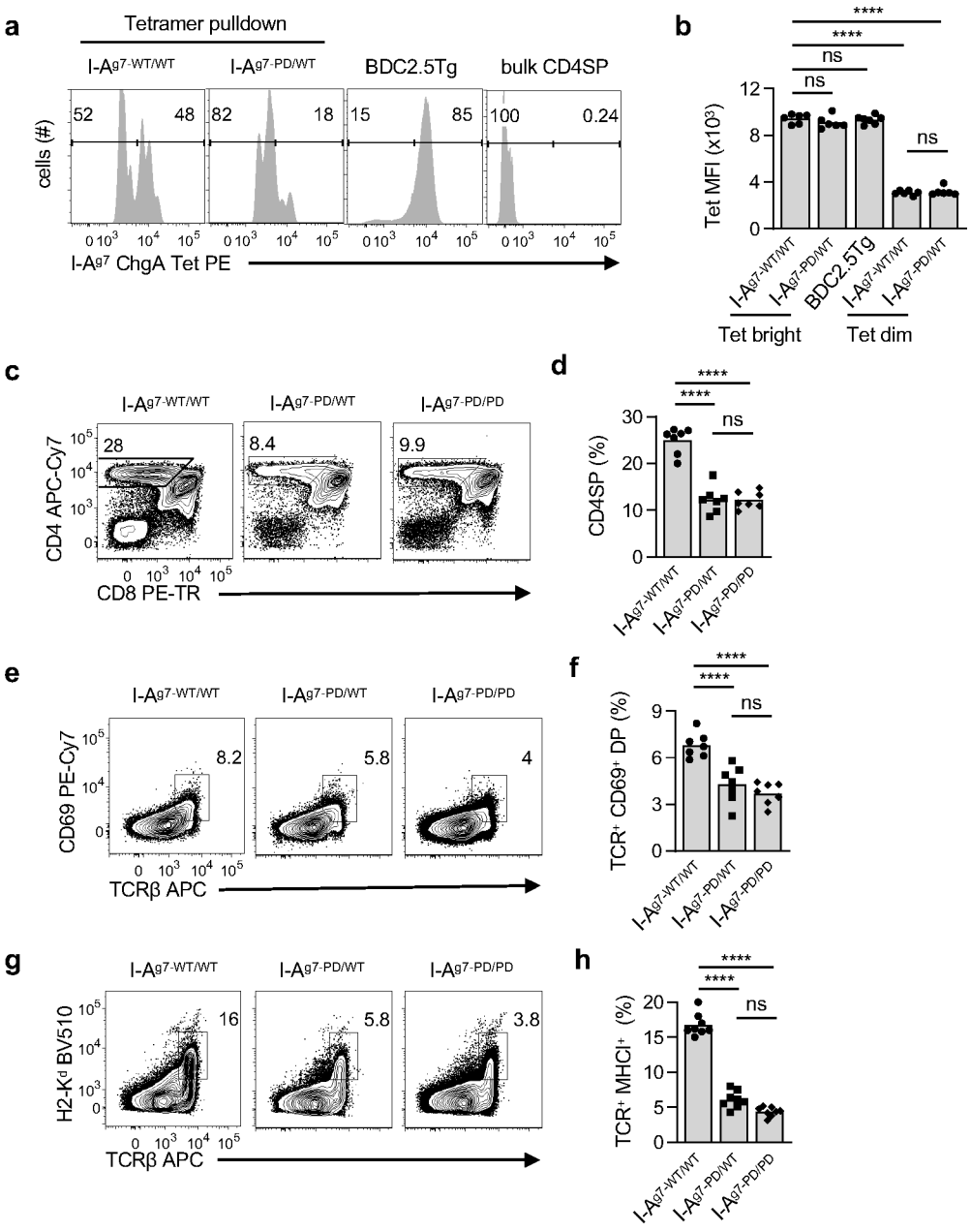

Extended Data Fig. 4. Expression of I-$A^{g7\text{-}PD}$ induces non-cognate negative selection of IA^{g7}-$ChgA_{HIP}$ reactive BDC2.5 TCR Tg thymocytes at the DP to SP transition.

(**a**) Flow cytometric analysis of IA^{g7}-$ChgA_{HIP}$ tetramer staining of CD4SP thymocytes following tetramer-based enrichment, isolated from I-$A^{g7\text{-}WT/WT}$, I-$A^{g7\text{-}PD/WT}$ mice or BDC2.5 TCR Tg on an I-$A^{g7\text{-}WT/WT}$ genetic background, or polyclonal CD4SP thymocyte without enrichment. (**b**) quantification of mean fluorescence intensity (MFI) of $tetramer^{bright}$ and $tetramer^{dim}$ populations of CD4SP thymocytes for each mouse strain. (**c-h**) BDC2.5 TCR Tg thymocytes undergo negative selection at the DP to CD4SP transition. (**c**) Flow cytometric analysis of CD4 and CD8-expressing thymocyte subsets from 6 weeks old BDC2.5 TCR Tg mice on a I-$A^{g7\text{-}WT/WT}$ (n=7), I-$A^{g7\text{-}PD/WT}$ (n=7) or I-$A^{g7\text{-}PD/PD}$ (n=7) genetic backgrounds, and (**d**) quantification of CD4SP thymocyte frequency. (**e**) Representative examples and (**f**) quantification of $CD4^+CD8^+$ thymocytes expressing CD69 and high levels of TCRβ. (**g**) Representative examples and (**h**) quantification of frequency at which BDC2.5 TCR Tg mice matured thymocytes into T cells, based on expression of MHCI and high levels of TCRβ. ns $P>0.05$; **** $P<0.0001$ (one-way ANOVA with Tukeys multiple comparisons test).

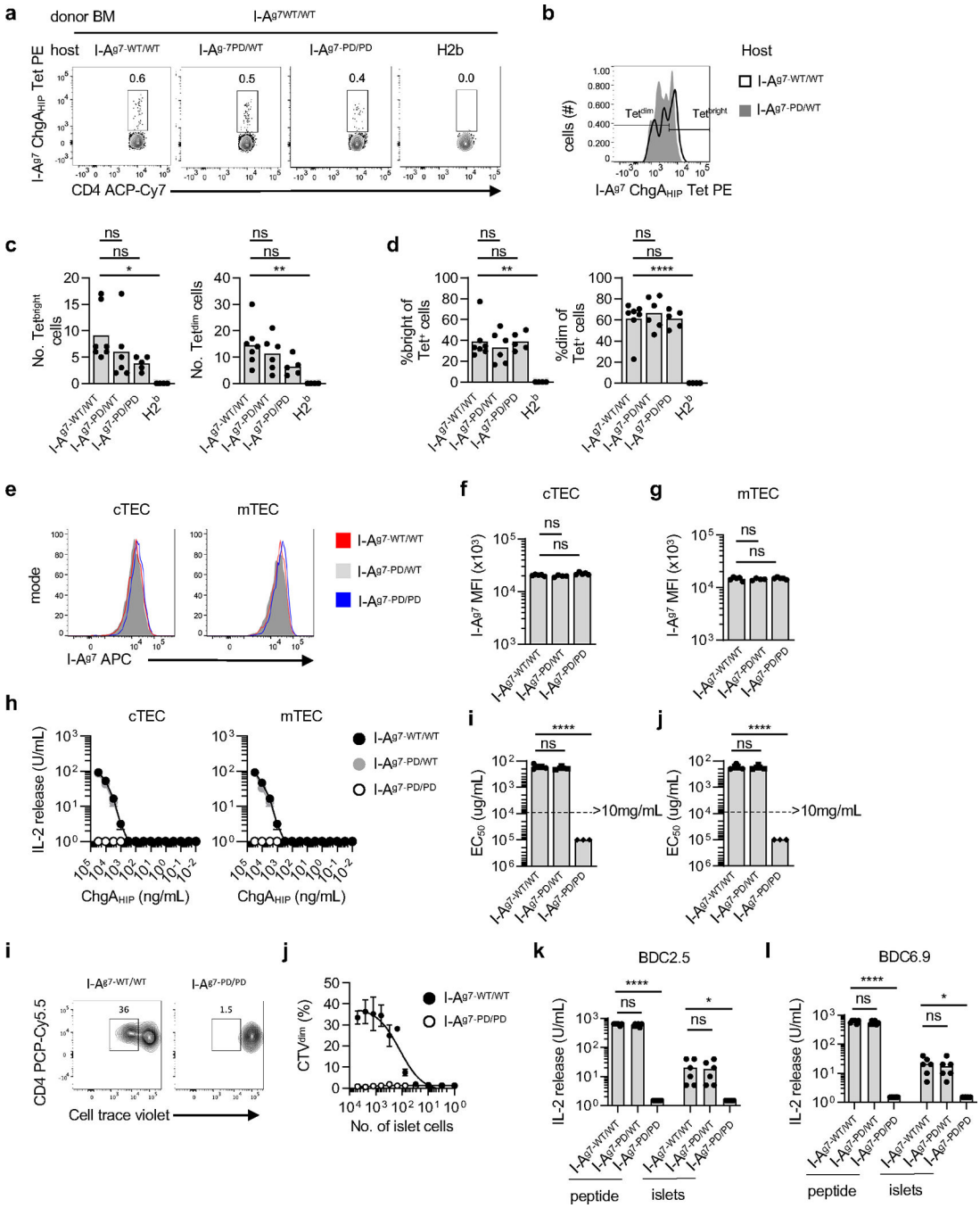

Extended Data Fig. 5. Expression of I-A$^{g7\text{-}WT/WT}$ on bone marrow derived cells allows development of mature I-A^{g7}-ChgA$_{HIP}$ tetramer^{bright} thymocytes.

(**a**) Representative staining from concatenated data (n=2 mice) of CD4SP thymocytes from radiation chimeras of I-A$^{g7\text{-}WT/WT}$ bone marrow (BM) into I-A$^{g7\text{-}WT/WT}$, I-A$^{g7\text{-}PD/WT,}$ I-A$^{g7\text{-}PD/PD}$ or H2^{b} expressing mice. (**b**) Overlay of I-A^{g7}-ChgA$_{HIP}$ tetramer^{+} CD4SP thymoctes from I-A$^{g7\text{-}WT/WT}$ and I-A$^{g7\text{-}PD/WT}$ chimeras with I-A$^{g7\text{-}WT/WT}$ BM. (**c**,**d**) Quantification of the (c) number and (d) percentage of I-A^{g7}-ChgA$_{HIP}$ tetramer^{bright} and tetramer^{dim} cells among individual I-A$^{g7\text{-}WT/WT}$ BM chimeric mice. (**e**) Overlay and (**f**,**g**)

MFI of I-A^{g7} staining on cortical and medullary thymic epithelial cells of 6 weeks old I-$A^{g7\text{-}WT/WT}$ (n=5), I-$A^{g7\text{-}PD/WT}$ (n=4), I-$A^{g7\text{-}PD/PD}$ (n=5) mice. (h) IL-2 release from BDC2.5 T cells hybridomas with co-cultured with $ChgA_{HIP}$ peptide and sorted cTECs and mTECs populations from I-$A^{g7\text{-}WT/WT}$, I-$A^{g7\text{-}PD/WT,}$ I-$A^{g7\text{-}PD/PD}$ mice. (**i**) Example and (**j**) quantification of BDC2.5 CD4 T cells proliferating in response to BM-DCs derived from I-$A^{g7\text{-}WT/WT}$ and I-$A^{g7\text{-}PD/PD}$ presenting β-islet cell preparations from replicate wells of two separate experiments, error bars are SEM. (**k**,**l**) Quantification of IL-2 release by BDC2.5 and BDC6.9 T cell hybridomas in response to BM-DCs derived from I-$A^{g7\text{-}WT/WT}$ and I-$A^{g7\text{-}PD/PD}$ presenting β-islet cell preparations or soluble peptide. Bars are mean values from 2 replicate experiments with triplicate wells. ns $P>0.05$; * $P<0.05$; ** $P<0.01$; **** $P<0.0001$ (one-way ANOVA with Dunnett's multiple comparisons test)

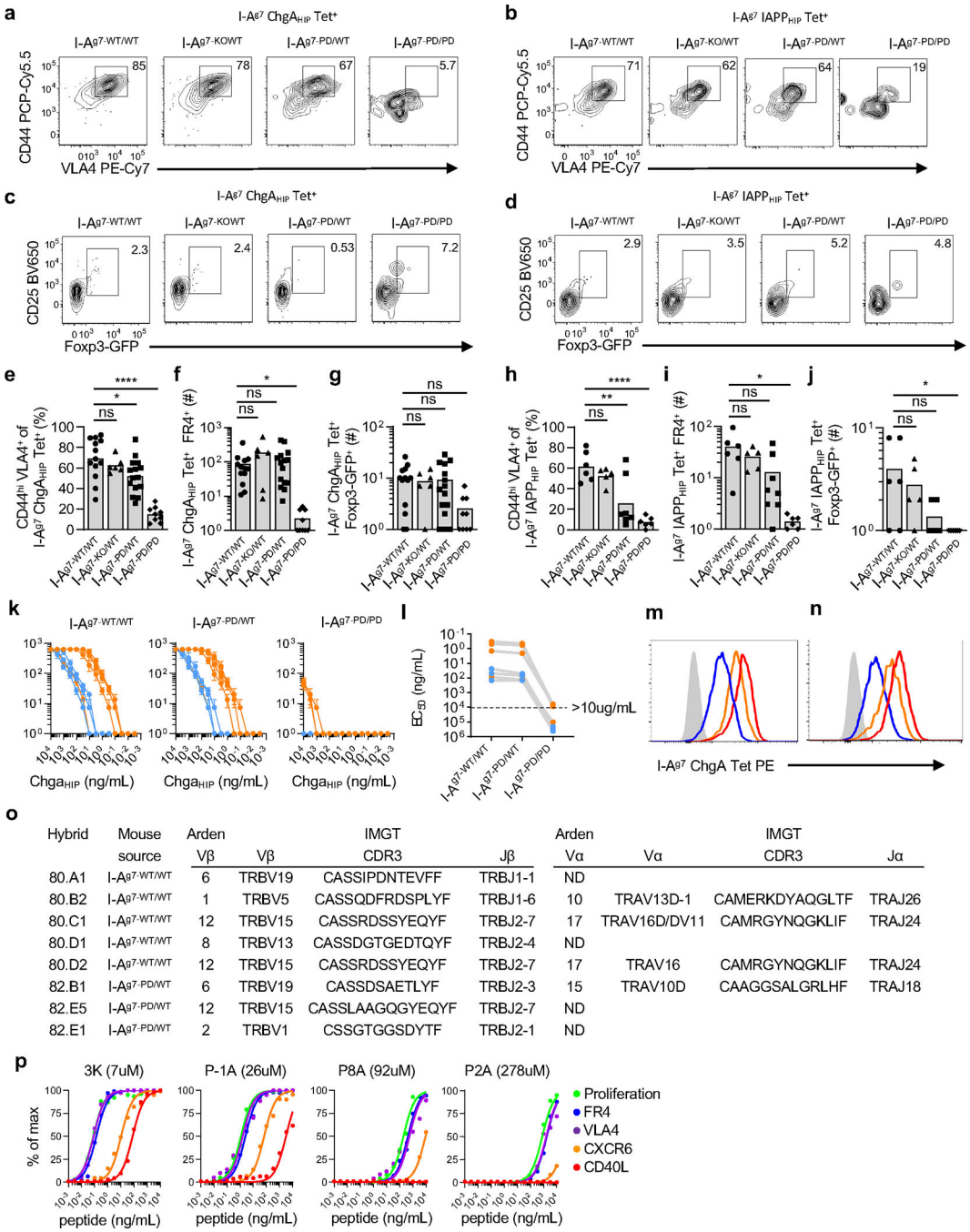

o

Hybrid	Mouse source	Arden Vβ	IMGT Vβ	IMGT CDR3	IMGT Jβ	Arden Vα	IMGT Vα	IMGT CDR3	IMGT Jα
80.A1	I-Aᵍ⁷-WT/WT	6	TRBV19	CASSIPDNTEVFF	TRBJ1-1	ND			
80.B2	I-Aᵍ⁷-WT/WT	1	TRBV5	CASSQDFRDSPLYF	TRBJ1-6	10	TRAV13D-1	CAMERKDYAQGLTF	TRAJ26
80.C1	I-Aᵍ⁷-WT/WT	12	TRBV15	CASSRDSSYEQYF	TRBJ2-7	17	TRAV16D/DV11	CAMRGYNQGKLIF	TRAJ24
80.D1	I-Aᵍ⁷-WT/WT	8	TRBV13	CASSDGTGEDTQYF	TRBJ2-4	ND			
80.D2	I-Aᵍ⁷-WT/WT	12	TRBV15	CASSRDSSYEQYF	TRBJ2-7	17	TRAV16	CAMRGYNQGKLIF	TRAJ24
82.B1	I-Aᵍ⁷-PD/WT	6	TRBV19	CASSDSAETLYF	TRBJ2-3	15	TRAV10D	CAAGGSALGRLHF	TRAJ18
82.E5	I-Aᵍ⁷-PD/WT	12	TRBV15	CASSLAAGQGYEQYF	TRBJ2-7	ND			
82.E1	I-Aᵍ⁷-PD/WT	2	TRBV1	CSSGTGGSDYTF	TRBJ2-1	ND			

Extended Data Fig. 6. Expression of IA$^{g7\text{-}PD}$ does not result in the differentiation of β-islet specific CD4 T cells into Foxp3^{+} Tregs.

(**a,b**) Flow cytometric analysis of CD44 and VLA4 on (**a**) I-A^{g7}-ChgA$_{HIP}$- and (**b**) I-A^{g7}-IAPP$_{HIP}$-specific CD4 T cells. (**c,d**) Flow cytometric analysis of Foxp3-gfp and CD25 on (**c**) I-A^{g7}-ChgA$_{HIP}$- and (**d**) I-A^{g7}-IAPP$_{HIP}$-specific CD4 T cells. Quantification of (**e,h**) CD44 and VLA4 expression, (**f,i**) FR4 expression and (**g,j**) Foxp3-gfp expression on (**e-g**) I-A^{g7}-ChgA and (**h-j**) I-A^{g7}-IAPP specific CD4 T cells isolated from I-A$^{g7\text{-}WT/WT}$ (n=13, 6), I-A$^{g7\text{-}KO/WT}$ (n=6, 6), I-A$^{g7\text{-}PD/WT}$ (n=15, 7) and I-A$^{g7\text{-}PD/PD}$ (n=9, 6) mice,

respectively. ns $P>0.05$; * $P<0.05$; ** $P<0.01$; **** $P<0.0001$ (one-way ANOVA with Tukeys multiple comparisons test). (**k,l**) Activation and quantification of EC_{50} values of $ChgA_{HIP}$-reactive T cell hybridomas in response to titrating amounts of $ChgA_{HIP}$ peptide co-cultured with I-$A^{g7\text{-}WT/WT}$, I-$A^{g7\text{-}PD/WT}$, I-$A^{g7\text{-}PD/PD}$ splenocytes. (**m, o**) I-A^{g7}-$ChgA_{HIP}$ tetramer binding of (m) T cell hybridomas 80.B2 (red), 80.C1 (orange) and 82.B1 (blue), (n) T cell transfectomas 80.B2 (red), 80.C1 (orange) and 82.B1 (blue). T cell hybridomas, and T cell transfectomas expressed similar levels of TCR. (**o**) TCR Vα and Vβ sequences from I-A^{g7}-$ChgA_{HIP}$-reactive hybridomas isolated from I-$A^{g7\text{-}WT/WT}$, I-$A^{g7\text{-}PD/WT}$ mice. (**p**) Influence of TCR:pMHC affinity and antigen concentration on CD4 T cell effector functions. B3K506 TCR T cells were activated with titrating concentrations of strong (3K; K_D = 7mM), medium (P-1A; K_D = 26mM), weak (P8A; K_D = 92mM) and very weak (P2A; K_D = 278mM) affinity ligands and expression of CD40L, CXCR6, VLA4 and FR4 was evaluated, as well as cellular proliferation.

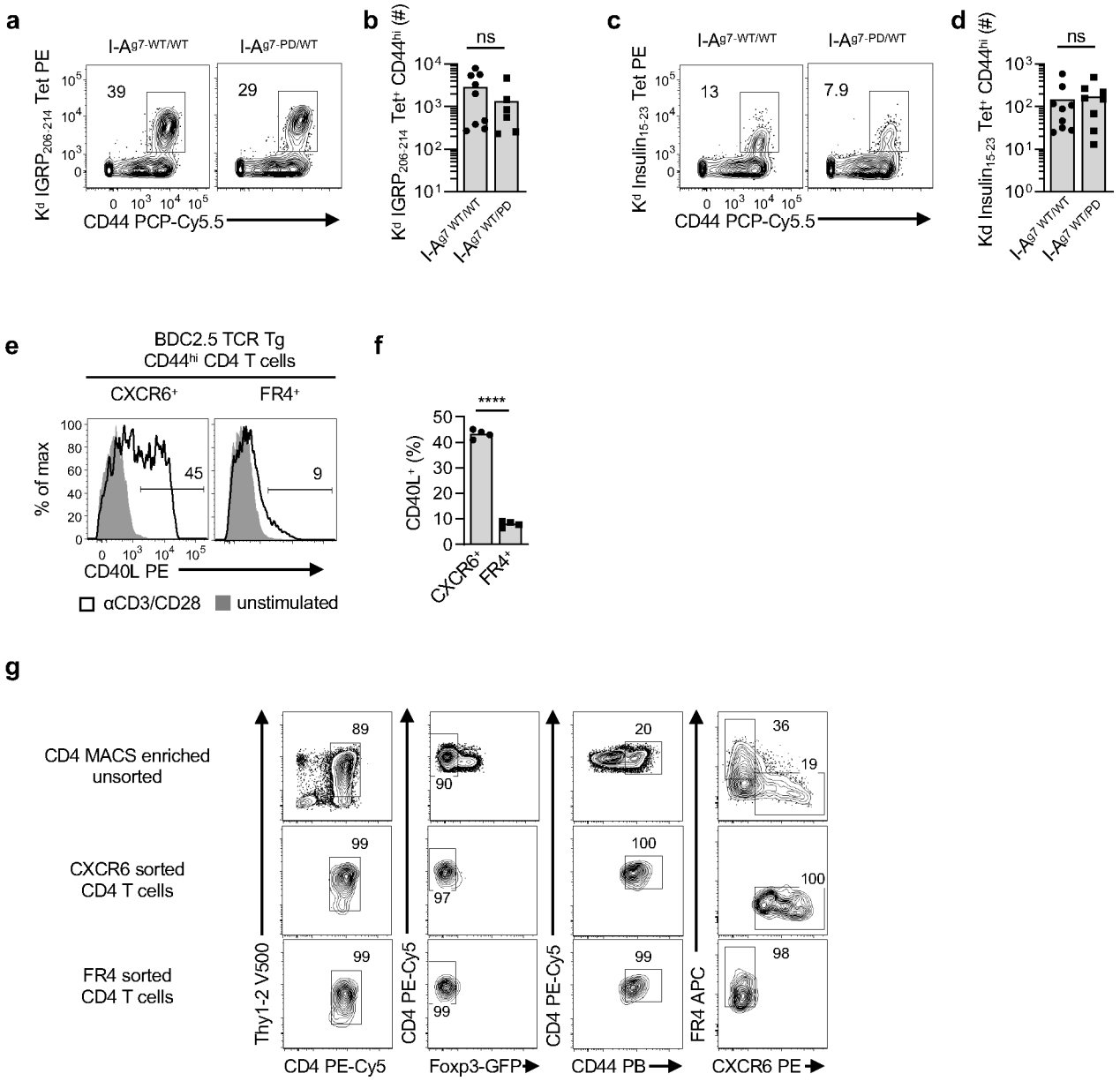

Extended Data Fig. 7. I-A$^{g7\text{-}PD}$ expressing mice can expand high frequencies of K^{d}-IGRP$_{206–214}$ and K^{d}-Insulin$_{15–23}$ specific CD8 T cells following viral activation.

(**a,b**) Flow cytometric analysis and quantification of K^{d}-IGRP$_{206–214}$ and (**c,d**) K^{d}-Insulin$_{15–23}$ specific CD8 T cells following tetramer-based enrichment, isolated from I-A$^{g7\text{-}WT/WT}$ (n=9, 9), I-A$^{g7\text{-}PD/WT}$ (n= 6, 9) mice infected with VSV-IGRP$_{206–214}$ or VSV-Insulin$_{15–23}$, respectively. (**e**) Flow cytometric analysis and (**f**) quantification of CD40L expression on CXCR6^{+} and FR4^{+} CD4 T cells from BDC2.5 TCR Tg mice following 4hrs *in vitro* stimulation with anti-CD3/CD28. ns P>0.05; **** P<0.0001 (unpaired two-tailed t test). (**g**) Purity of flow cytometry sorting of mouse CXCR6^{+} and FR4^{+} T cells for adoptive transfer.

Acknowledgments

Supported by the US National Institutes of Health (AI143976 and AR071269) to E.S.H. S.B.C. was supported by an NIH training grant (5T32A1007349–31).

References

1. Eisenbarth GS Type I diabetes mellitus. A chronic autoimmune disease. N Engl J Med 314, 1360–1368 (1986). [PubMed: 3517648]
2. Ziegler AG & Nepom GT Prediction and pathogenesis in type 1 diabetes. Immunity 32, 468–478 (2010). [PubMed: 20412757]
3. Herold KC, Vignali DA, Cooke A & Bluestone JA Type 1 diabetes: translating mechanistic observations into effective clinical outcomes. Nat Rev Immunol 13, 243–256 (2013). [PubMed: 23524461]
4. Bendelac A, Carnaud C, Boitard C & Bach JF Syngeneic transfer of autoimmune diabetes from diabetic NOD mice to healthy neonates. Requirement for both L3T4+ and Lyt-2+ T cells. J Exp Med 166, 823–832 (1987). [PubMed: 3309126]
5. Serreze DV et al. B lymphocytes are essential for the initiation of T cell-mediated autoimmune diabetes: analysis of a new “speed congenic” stock of NOD.Ig mu null mice. J Exp Med 184, 2049–2053 (1996). [PubMed: 8920894]
6. Carrero JA et al. Resident macrophages of pancreatic islets have a seminal role in the initiation of autoimmune diabetes of NOD mice. Proc Natl Acad Sci U S A 114, E10418–E10427 (2017). [PubMed: 29133420]
7. Anderson MS & Bluestone JA The NOD mouse: a model of immune dysregulation. Annu Rev Immunol 23, 447–485 (2005). [PubMed: 15771578]
8. Atkinson MA & Maclaren NK The pathogenesis of insulin-dependent diabetes mellitus. N Engl J Med 331, 1428–1436 (1994). [PubMed: 7969282]
9. Todd JA Etiology of type 1 diabetes. Immunity 32, 457–467 (2010). [PubMed: 20412756]
10. Todd JA, Bell JI & McDevitt HO HLA-DQ beta gene contributes to susceptibility and resistance to insulin-dependent diabetes mellitus. Nature 329, 599–604 (1987). [PubMed: 3309680]
11. Acha-Orbea H & McDevitt HO The first external domain of the nonobese diabetic mouse class II I-A beta chain is unique. Proc Natl Acad Sci U S A 84, 2435–2439 (1987). [PubMed: 2882518]
12. Corper AL et al. A structural framework for deciphering the link between I-Ag7 and autoimmune diabetes. Science 288, 505–511 (2000). [PubMed: 10775108]
13. Latek RR et al. Structural basis of peptide binding and presentation by the type I diabetes-associated MHC class II molecule of NOD mice. Immunity 12, 699–710 (2000). [PubMed: 10894169]
14. Stadinski B, Kappler J & Eisenbarth GS Molecular targeting of islet autoantigens. Immunity 32, 446–456 (2010). [PubMed: 20412755]
15. Unanue ER Antigen presentation in the autoimmune diabetes of the NOD mouse. Annu Rev Immunol 32, 579–608 (2014). [PubMed: 24499272]
16. Gioia L et al. Position beta57 of I-A(g7) controls early anti-insulin responses in NOD mice, linking an MHC susceptibility allele to type 1 diabetes onset. Science immunology 4 (2019).
17. Santos Martin JL et al. Different statistical models used in the calculation of the prevalence of insulin-dependent diabetes mellitus according to the polymorphism of the HLA-DQ region. Immunol Cell Biol 75, 351–355 (1997). [PubMed: 9315476]
18. Dendrou CA, Petersen J, Rossjohn J & Fugger L HLA variation and disease. Nat Rev Immunol 18, 325–339 (2018). [PubMed: 29292391]
19. Latorre D et al. T cells in patients with narcolepsy target self-antigens of hypocretin neurons. Nature 562, 63–68 (2018). [PubMed: 30232458]
20. Hu X et al. Additive and interaction effects at three amino acid positions in HLA-DQ and HLA-DR molecules drive type 1 diabetes risk. Nat Genet 47, 898–905 (2015). [PubMed: 26168013]

21. Wicker LS, Miller BJ, Chai A, Terada M & Mullen Y Expression of genetically determined diabetes and insulitis in the nonobese diabetic (NOD) mouse at the level of bone marrow-derived cells. Transfer of diabetes and insulitis to nondiabetic (NOD X B10) F1 mice with bone marrow cells from NOD mice. J Exp Med 167, 1801–1810 (1988). [PubMed: 3290380]
22. Wicker LS et al. Autoimmune syndromes in major histocompatibility complex (MHC) congenic strains of nonobese diabetic (NOD) mice. The NOD MHC is dominant for insulitis and cyclophosphamide-induced diabetes. J Exp Med 176, 67–77 (1992). [PubMed: 1613467]
23. Hattori M et al. The Nod Mouse - Recessive Diabetogenic Gene in the Major Histocompatibility Complex. Science 231, 733–735 (1986). [PubMed: 3003909]
24. Lund T et al. Prevention of insulin-dependent diabetes mellitus in non-obese diabetic mice by transgenes encoding modified I-A beta-chain or normal I-E alpha-chain. Nature 345, 727–729 (1990). [PubMed: 2163026]
25. Singer SM et al. Prevention of diabetes in NOD mice by a mutated I-Ab transgene. Diabetes 47, 1570–1577 (1998). [PubMed: 9753294]
26. Tsai S & Santamaria P MHC Class II Polymorphisms, Autoreactive T-Cells, and Autoimmunity. Front Immunol 4, 321 (2013). [PubMed: 24133494]
27. Ooi JD et al. Dominant protection from HLA-linked autoimmunity by antigen-specific regulatory T cells. Nature 545, 243–247 (2017). [PubMed: 28467828]
28. Tsai S et al. Antidiabetogenic MHC class II promotes the differentiation of MHC-promiscuous autoreactive T cells into FOXP3+ regulatory T cells. Proc Natl Acad Sci U S A 110, 3471–3476 (2013). [PubMed: 23401506]
29. Gregersen JW et al. Functional epistasis on a common MHC haplotype associated with multiple sclerosis. Nature 443, 574–577 (2006). [PubMed: 17006452]
30. Stadinski BD et al. A temporal thymic selection switch and ligand binding kinetics constrain neonatal Foxp3+ Treg cell development. Nat Immunol 20, 1046–1058 (2019). [PubMed: 31209405]
31. Zakharov PN, Hu H, Wan X & Unanue ER Single-cell RNA sequencing of murine islets shows high cellular complexity at all stages of autoimmune diabetes. J Exp Med 217 (2020).
32. Kim CH et al. Bonzo/CXCR6 expression defines type 1-polarized T-cell subsets with extralymphoid tissue homing potential. J Clin Invest 107, 595–601 (2001). [PubMed: 11238560]
33. Kalekar LA et al. CD4(+) T cell anergy prevents autoimmunity and generates regulatory T cell precursors. Nat Immunol 17, 304–314 (2016). [PubMed: 26829766]
34. Stadinski BD et al. Hydrophobic CDR3 residues promote the development of self-reactive T cells. Nat Immunol 17, 946–955 (2016). [PubMed: 27348411]
35. Stadinski BD et al. Chromogranin A is an autoantigen in type 1 diabetes. Nat Immunol 11, 225–231 (2010). [PubMed: 20139986]
36. Delong T et al. Pathogenic CD4 T cells in type 1 diabetes recognize epitopes formed by peptide fusion. Science 351, 711–714 (2016). [PubMed: 26912858]
37. Wan X et al. The MHC-II peptidome of pancreatic islets identifies key features of autoimmune peptides. Nat Immunol (2020).
38. Govern CC, Paczosa MK, Chakraborty AK & Huseby ES Fast on-rates allow short dwell time ligands to activate T cells. Proc Natl Acad Sci U S A 107, 8724–8729 (2010). [PubMed: 20421471]
39. Baron JL, Reich EP, Visintin I & Janeway CA Jr. The pathogenesis of adoptive murine autoimmune diabetes requires an interaction between alpha 4-integrins and vascular cell adhesion molecule-1. J Clin Invest 93, 1700–1708 (1994). [PubMed: 7512990]
40. Ferris ST et al. cDC1 prime and are licensed by CD4(+) T cells to induce anti-tumour immunity. Nature 584, 624–629 (2020). [PubMed: 32788723]
41. Ridge JP, Di Rosa F & Matzinger P A conditioned dendritic cell can be a temporal bridge between a CD4+ T-helper and a T-killer cell. Nature 393, 474–478 (1998). [PubMed: 9624003]
42. Schoenberger SP, Toes RE, van der Voort EI, Offringa R & Melief CJ T-cell help for cytotoxic T lymphocytes is mediated by CD40-CD40L interactions. Nature 393, 480–483 (1998). [PubMed: 9624005]

43. Bennett SR et al. Help for cytotoxic-T-cell responses is mediated by CD40 signalling. Nature 393, 478–480 (1998). [PubMed: 9624004]
44. Wong FS et al. Identification of an MHC class I-restricted autoantigen in type 1 diabetes by screening an organ-specific cDNA library. Nat Med 5, 1026–1031 (1999). [PubMed: 10470079]
45. Lieberman SM et al. Identification of the beta cell antigen targeted by a prevalent population of pathogenic CD8+ T cells in autoimmune diabetes. Proc Natl Acad Sci U S A 100, 8384–8388 (2003). [PubMed: 12815107]
46. Hogquist KA & Jameson SC The self-obsession of T cells: how TCR signaling thresholds affect fate 'decisions' and effector function. Nat Immunol 15, 815–823 (2014). [PubMed: 25137456]
47. Huseby ES & Teixeiro E The perception and response of T cells to a changing environment are based on the law of initial value. Sci Signal 15, eabj9842 (2022). [PubMed: 35639856]
48. Felix NJ & Allen PM Specificity of T-cell alloreactivity. Nat Rev Immunol 7, 942–953 (2007). [PubMed: 18007679]
49. Yagi J & Janeway CA Jr. Ligand thresholds at different stages of T cell development. Int Immunol 2, 83–89 (1990). [PubMed: 2150922]
50. Davey GM et al. Preselection thymocytes are more sensitive to T cell receptor stimulation than mature T cells. J Exp Med 188, 1867–1874 (1998). [PubMed: 9815264]
51. Lucas B, Stefanova I, Yasutomo K, Dautigny N & Germain RN Divergent changes in the sensitivity of maturing T cells to structurally related ligands underlies formation of a useful T cell repertoire. Immunity 10, 367–376 (1999). [PubMed: 10204492]
52. Li QJ et al. miR-181a is an intrinsic modulator of T cell sensitivity and selection. Cell 129, 147–161 (2007). [PubMed: 17382377]
53. Sant'Angelo DB & Janeway CA Jr. Negative selection of thymocytes expressing the D10 TCR. Proc Natl Acad Sci U S A 99, 6931–6936 (2002). [PubMed: 12011450]
54. Suri A, Walters JJ, Gross ML & Unanue ER Natural peptides selected by diabetogenic DQ8 and murine I-A(g7) molecules show common sequence specificity. J Clin Invest 115, 2268–2276 (2005). [PubMed: 16075062]
55. Kishimoto H & Sprent J Negative selection in the thymus includes semimature T cells. J Exp Med 185, 263–271 (1997). [PubMed: 9016875]
56. Daley SR, Hu DY & Goodnow CC Helios marks strongly autoreactive CD4+ T cells in two major waves of thymic deletion distinguished by induction of PD-1 or NF-kappaB. J Exp Med 210, 269–285 (2013). [PubMed: 23337809]
57. Klein L, Robey EA & Hsieh CS Central CD4(+) T cell tolerance: deletion versus regulatory T cell differentiation. Nat Rev Immunol 19, 7–18 (2019). [PubMed: 30420705]
58. Zhang Y et al. In situ beta cell death promotes priming of diabetogenic CD8 T lymphocytes. J Immunol 168, 1466–1472 (2002). [PubMed: 11801690]
59. Krishnamurthy B et al. Responses against islet antigens in NOD mice are prevented by tolerance to proinsulin but not IGRP. J Clin Invest 116, 3258–3265 (2006). [PubMed: 17143333]
60. Amrani A et al. CD154-dependent priming of diabetogenic CD4(+) T cells dissociated from activation of antigen-presenting cells. Immunity 16, 719–732 (2002). [PubMed: 12049723]
61. Wan X & Unanue ER Unique features in the presentation of insulin epitopes in autoimmune diabetes: an update. Curr Opin Immunol 46, 30–37 (2017). [PubMed: 28456018]
62. Ferris ST et al. A minor subset of Batf3-dependent antigen-presenting cells in islets of Langerhans is essential for the development of autoimmune diabetes. Immunity 41, 657–669 (2014). [PubMed: 25367577]
63. Ruedl C, Bachmann MF & Kopf M The antigen dose determines T helper subset development by regulation of CD40 ligand. Eur J Immunol 30, 2056–2064 (2000). [PubMed: 10940895]
64. Stadinski BD et al. A role for differential variable gene pairing in creating T cell receptors specific for unique major histocompatibility ligands. Immunity 35, 694–704 (2011). [PubMed: 22101158]
65. Wong FS, Moustakas AK, Wen L, Papadopoulos GK & Janeway CA Jr. Analysis of structure and function relationships of an autoantigenic peptide of insulin bound to H-2K(d) that stimulates CD8 T cells in insulin-dependent diabetes mellitus. Proc Natl Acad Sci U S A 99, 5551–5556 (2002). [PubMed: 11943852]

66. Huseby ES, Crawford F, White J, Kappler J & Marrack P Negative selection imparts peptide specificity to the mature T cell repertoire. Proc Natl Acad Sci U S A 100, 11565–11570 (2003). [PubMed: 14504410]

67. Yang X et al. TCRklass: a new K-string-based algorithm for human and mouse TCR repertoire characterization. J Immunol 194, 446–454 (2015). [PubMed: 25404364]

68. Love MI, Huber W & Anders S Moderated estimation of fold change and dispersion for RNA-seq data with DESeq2. Genome biology 15, 550 (2014). [PubMed: 25516281]

69. Xing Y & Hogquist KA Isolation, identification, and purification of murine thymic epithelial cells. J Vis Exp, e51780 (2014). [PubMed: 25145384]

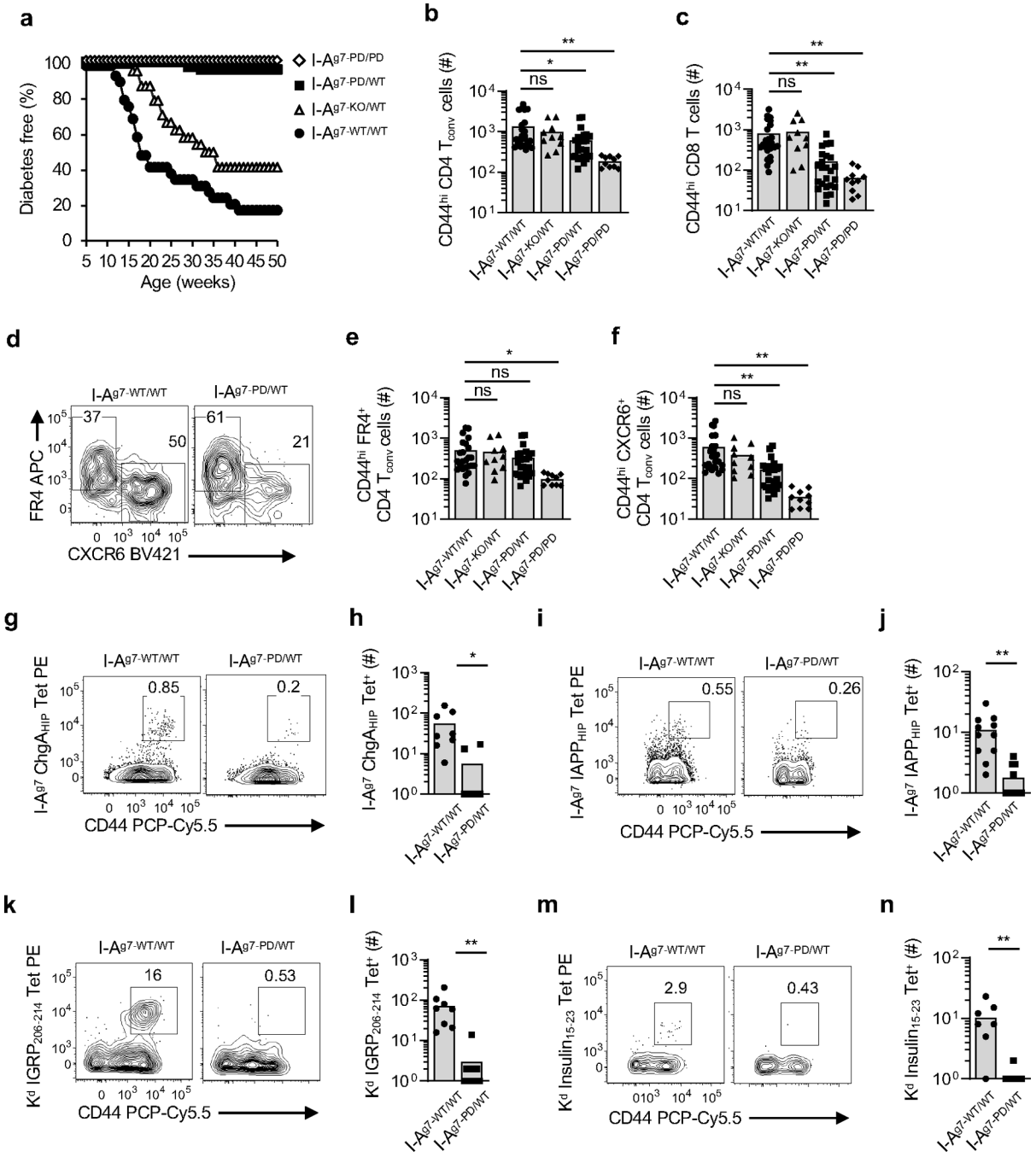

Fig. 1. Homozygous or hemizygous expression of I-A^{g7} is required for pancreas targeting by β-islet specific T cells and disease progression.

(**a**) Incidence of T1D in NOD mice carrying I-A$^{g7\ WT/WT}$ (n=29), I-A$^{g7\ KO/WT}$ (n=24), I-A$^{g7\ PD/WT}$ (n=61) or I-A$^{g7\ PD/PD}$ (n=21) alleles. (**b, c**) Quantification of polyclonal (**b**) CD44^{hi} CD4^{+} T cells and (c) CD44^{hi} CD8^{+} T cells within the pancreatic infiltrate of non-diabetic mice between 12–16 weeks of age (**d-f**) Representative examples of (**d**) CXCR6 and FR4 staining, and quantification of pancreas infiltrating CD44^{hi} CD4 T cells expressing (**e**) FR4 or (**f**) CXCR6. (**c-f**) I-A$^{g7\ WT/WT}$ (n=24), I-A$^{g7\ KO/WT}$ (n=10), I-A$^{g7\ PD/WT}$ (n=25)

or I-A$^{g7\ PD/PD}$ (n=10) ns P >0.05; * P <0.05; ** P < 0.01 (one-way ANOVA with Tukeys multiple comparisons test). (**g-n**) Example contour plots from concatenated datasets (n=2 mice) and quantification of β-islet-specific (**g-j**) CD4^{+} and (**k-n**) CD8^{+} T cells in I-A$^{g7\text{-}WT/WT}$ and I-A$^{g7\text{-}PD/WT}$ mice. Pancreatic infiltrate of I-A$^{g7\text{-}WT/WT}$ and I-A$^{g7\text{-}PD/WT}$ mice were stained with (**g, h**) I-A^{g7}-ChgA$_{HIP}$ tetramer, I-A$^{g7\ WT/WT}$ (n=8), I-A$^{g7\ PD/WT}$ (n=8) (**i, j**) I-A^{g7}-IAPP$_{HIP}$ tetramer, I-A$^{g7\ WT/WT}$ (n=11), I-A$^{g7\ PD/WT}$ (n=10) (**k, l**) K^{d}-IGRP$_{206–214}$, I-A$^{g7\ WT/WT}$ (n=8), I-A$^{g7\ PD/WT}$ (n=8) or (**m, n**) K^{d}-Insulin$_{15–23}$ I-A$^{g7\ WT/WT}$ (n=7), I-A$^{g7\ PD/WT}$ (n=7) and quantified. * P <0.05; ** P < 0.01 (unpaired two-tailed t-test).

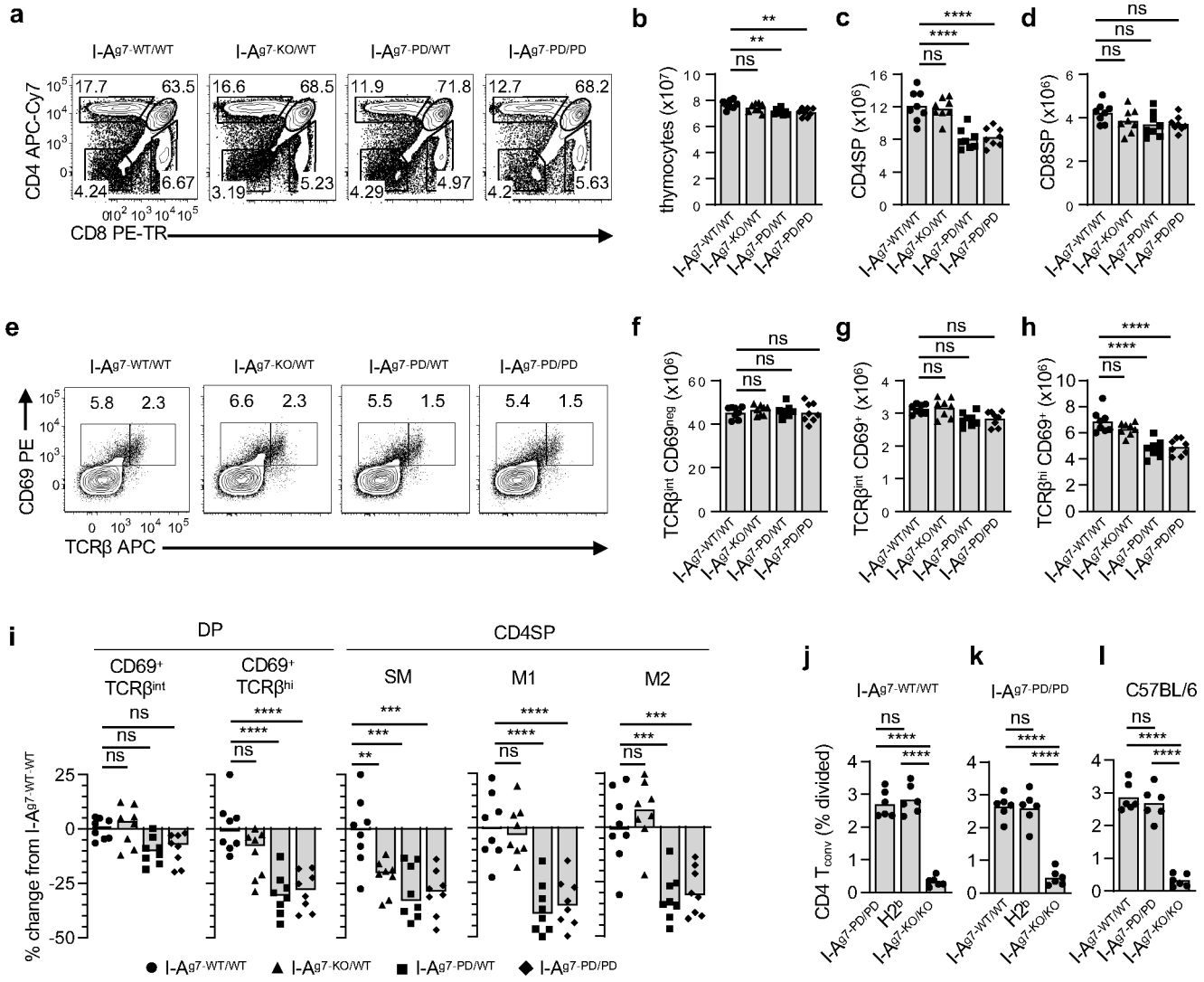

Fig. 2. I-A^{g7} β56/57 polymorphisms control thymic negative selection of CD4 T cells at the CD4^{+}CD8^{+} TCRβ^{int} to TCRβ^{hi} transition.

(**a**) Representative examples of CD4 and CD8-staining of thymocytes from individual 6 weeks old I-A$^{g7\text{-}WT/WT}$ (n=8), I-A$^{g7\text{-}KO/WT}$ (n=8), I-A$^{g7\text{-}PD/WT}$ (n=8) and I-A$^{g7\text{-}PD/PD}$ (n=8) mice show differential generation of CD4SP thymocytes. (**b**) Total number of thymocytes and (**c**) mature CD4 SP and (**d**) CD8SP thymocytes generated in each strain. (**e**) Representative examples of CD69 and TCRβ staining of CD4^{+}CD8^{+} thymocytes. (**f-h**) Total number of CD4^{+}CD8^{+} thymocytes that are (**f**) TCRβ^{int} and CD69^{neg}, (**g**) TCRβ^{int} and CD69^{pos} and (**h**) TCRβ^{hi} and CD69^{pos} that are generated in each strain. (**i**) Percent change in frequency of CD4^{+}CD8^{+} and CD4SP thymocyte subsets generated in each strain compared to I-A$^{g7\text{-}WT/WT}$ mice. (**j-l**) Frequency at which mature CD4 T cells isolated from (**j**) I-A$^{g7\text{-}WT/WT}$, (**k**) I-A$^{g7\text{-}PD/PD}$ and **(l)** C57BL/6 mice proliferate in response allogeneic APCs. ns P>0.05, ** P< 0.01; *** P< 0.001; **** P<0.0001 (one-way ANOVA with Tukeys multiple comparisons test).

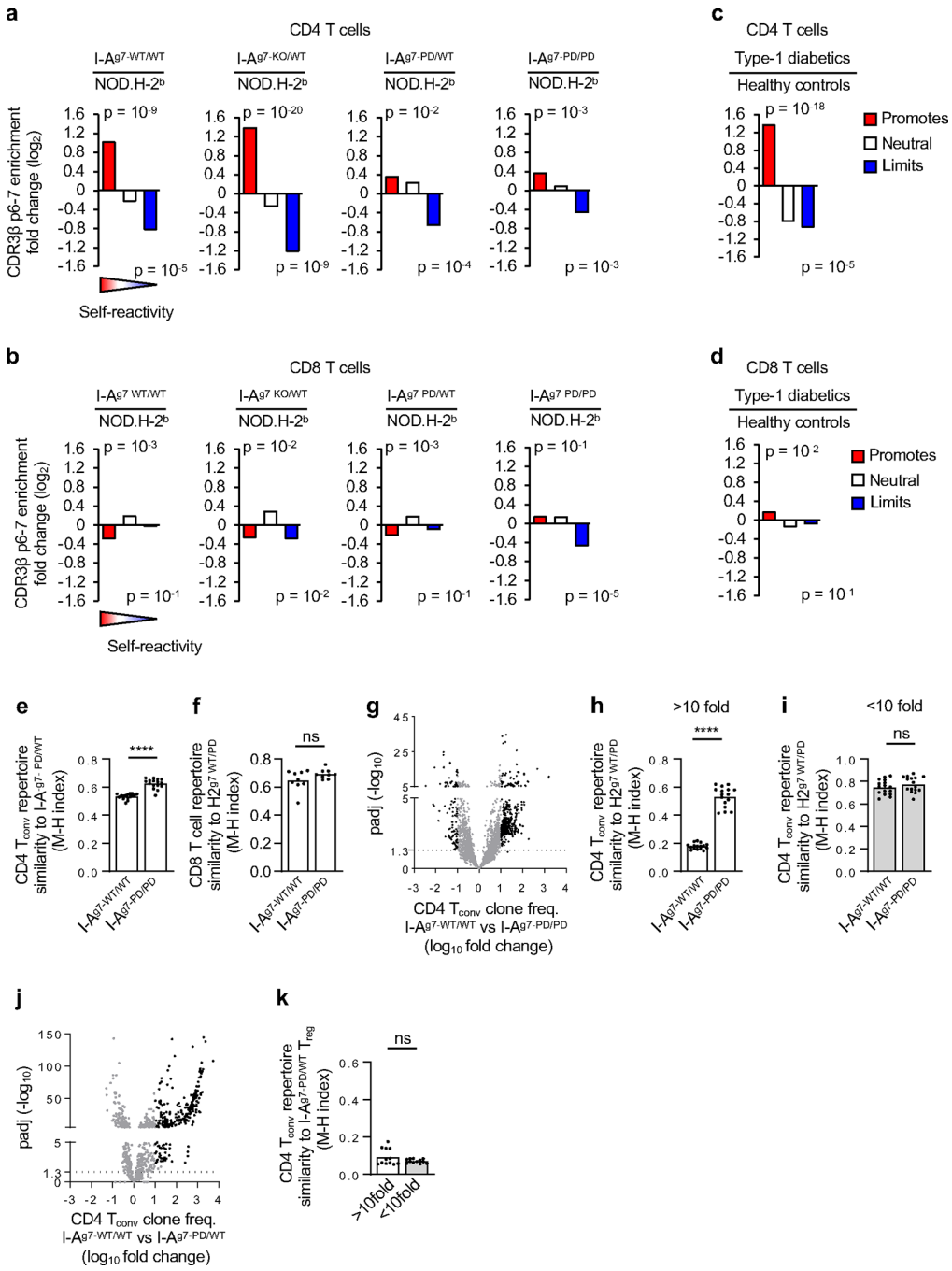

Fig. 3. Expression of I-A$^{g7\text{-}PD}$ has a dominant role in inducing T cell tolerance to the I-A^{g7}-restricted T cell repertoire.

(**a,b**) CD4$^+$ T cells in NOD mice with homozygous or hemizygous expression of I-A^{g7} are enriched in CDR3β P6–7 doublets that promote self-reactivity. Fold change in the number of differentially expressed doublets that promote (red), are neutral (white) or limit (blue) self-reactivity among naïve (a) CD4$^+$ or (b) CD8$^+$ T cells in 8 weeks old I-A$^{g7\text{-}WT/WT}$, I-A$^{g7\text{-}KO/WT}$, I-A$^{g7\text{-}PD/WT}$ and I-A$^{g7\text{-}PD/PD}$ mice as compared to NOD.H-2^b mice. (**c, d**) CD4$^+$ T cells in individuals with T1D are enriched in CDR3β P6–7 doublets that promote

self-reactivity. Fold change in the number of differentially expressed doublets that promote (red), are neutral (white) or limit (blue) self-reactivity among naïve (c) $CD4^+$ or (d) $CD8^+$ T cells in individuals with or without T1D (p values are the probability mass function of the hypergeometric distribution). (**e-i**) Expression of I-$A^{g7\text{-}PD}$ limits the development of I-A^{g7}-restricted CD4 T cells. (**e-f**) Morisita-Horn analysis of the 500 most frequent $V\alpha2^+$ clonotypes among (**e**) $CD4^+$ T_{conv} or (**f**) $CD8^+$ T cells from I-$A^{g7\text{-}WT/WT}$ and I-$A^{g7\text{-}PD/PD}$ mice in I-$A^{g7\text{-}PD/WT}$ mice (**g**) Volcano plot of clonal frequency difference between I-$A^{g7\text{-}WT/WT}$ and I-$A^{g7\text{-}PD/PD}$ mice for the 1000 most frequent $V\alpha2^+$ CD4 T_{conv} clonotypes present in I-$A^{g7\text{-}WT/WT}$ mice and the 1000 most frequent $V\alpha2^+$ CD4 T_{conv} clonotypes present in I-$A^{g7\text{-}PD/PD}$ mice. Clonotype frequencies with >10-fold differences are colored black. (**h**) Morisita-Horn analysis of clonotype usage in I-$A^{g7\text{-}PD/WT}$ mice for clonotypes >10-fold or (**i**) <10-fold enriched between I-$A^{g7\text{-}WT/WT}$ and I-$A^{g7\text{-}PD/PD}$ mice. (**j**) Volcano plot of the 1000 most frequent $Va2^+$ CD4 T_{conv} clonotypes present in I-$A^{g7\text{-}WT/WT}$ compared to their frequency in I-$A^{g7\text{-}PD/WT}$ mice. Clonotypes that are >10-fold decreased in I-$A^{g7\text{-}PD/WT}$ mice are colored black. (**k**) Morisita-Horn analysis of CD4 T_{conv} compared to $Foxp3^+$ CD4 Tregs for clonotypes that are >10-fold and <10-fold decreased in I-$A^{g7\text{-}PD/WT}$ mice. ns $P>0.05$; **** $P<0.0001$ (Mann-Whittney U test).

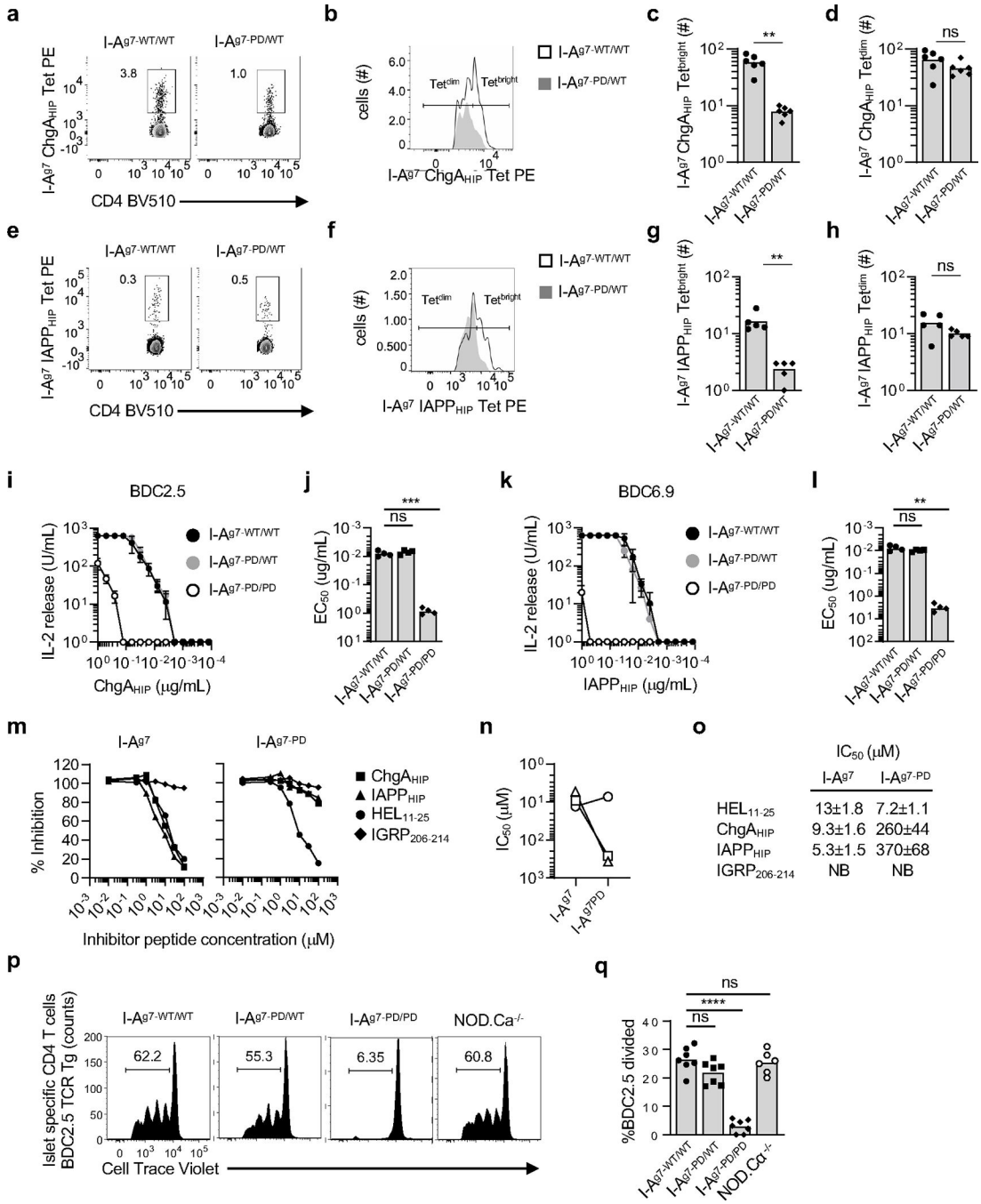

Fig. 4. Expression of I-A$^{g7\text{-}PD}$ induces non-cognate negative selection of tetramer^{bright} β-islet specific CD4$^+$ T cells.

(**a-h**) Representative examples of flow cytometric analysis of CD4$^+$ thymocytes from I-A$^{g7\text{-}WT/WT}$ and I-A$^{g7\text{-}PD/WT}$ mice at 6 weeks of age following (**a,b**) I-A^{g7}-ChgA$_{HIP}$ c and (**e,f**) I-A^{g7}-IAPP$_{HIP}$ pMHC tetramer-enrichment using concatenated datasets containing n=3 mice. (**c, d**) Quantification of TCRβ$^+$ tetramer$^+$ CD4SP thymocytes from individual mice that stain bright or dim with I-A^{g7}-ChgA (n=6) or (**g,h**) I-A^{g7}-IAPP tetramers (n=5). (**i-l**) Activation and quantification of EC$_{50}$ values of (**i,j**) BDC2.5 and (**k,l**) BDC6.9 CD4$^+$

T cell hybridomas in response to titrating amounts of $ChgA_{HIP}$ or $IAPP_{HIP}$ peptide. Data are average of replicate wells and are representative of two experiments. (**m-o**) Competitive peptide binding assay for $ChgA_{HIP}$, $IAPP_{HIP}$ $HEL_{11–25}$ and $IGRP_{206–214}$ peptides in competition with biotinylated $HEL_{11–25}$ for binding to I-A^{g7} and I-A^{g7PD}. (m) Representative analysis of individual competitive peptide binding assay. (n-o) Graph and table of average IC_{50} value from 4 replicate competitive peptide binding assays along with standard deviation, not bound (NB). (**p**) Flow cytometric analysis and (**q**) quantification of CTV-labelled $ChgA_{HIP}$ specific BDC2.5 CD4 T cells transferred into I-$A^{g7\text{-}WT/WT}$ (n=6), I-$A^{g7\text{-}PD/WT}$ (n=6), I-$A^{g7\text{-}PD/PD}$ (n=6) or NOD.$Ca^{-/-}$ (n=6) mice. T cell proliferation was analyzed for cells isolated from the pancLN. ns $P>0.05$, ****$P<0.0001$ (one-way ANOVA with Tukeys multiple comparisons test).

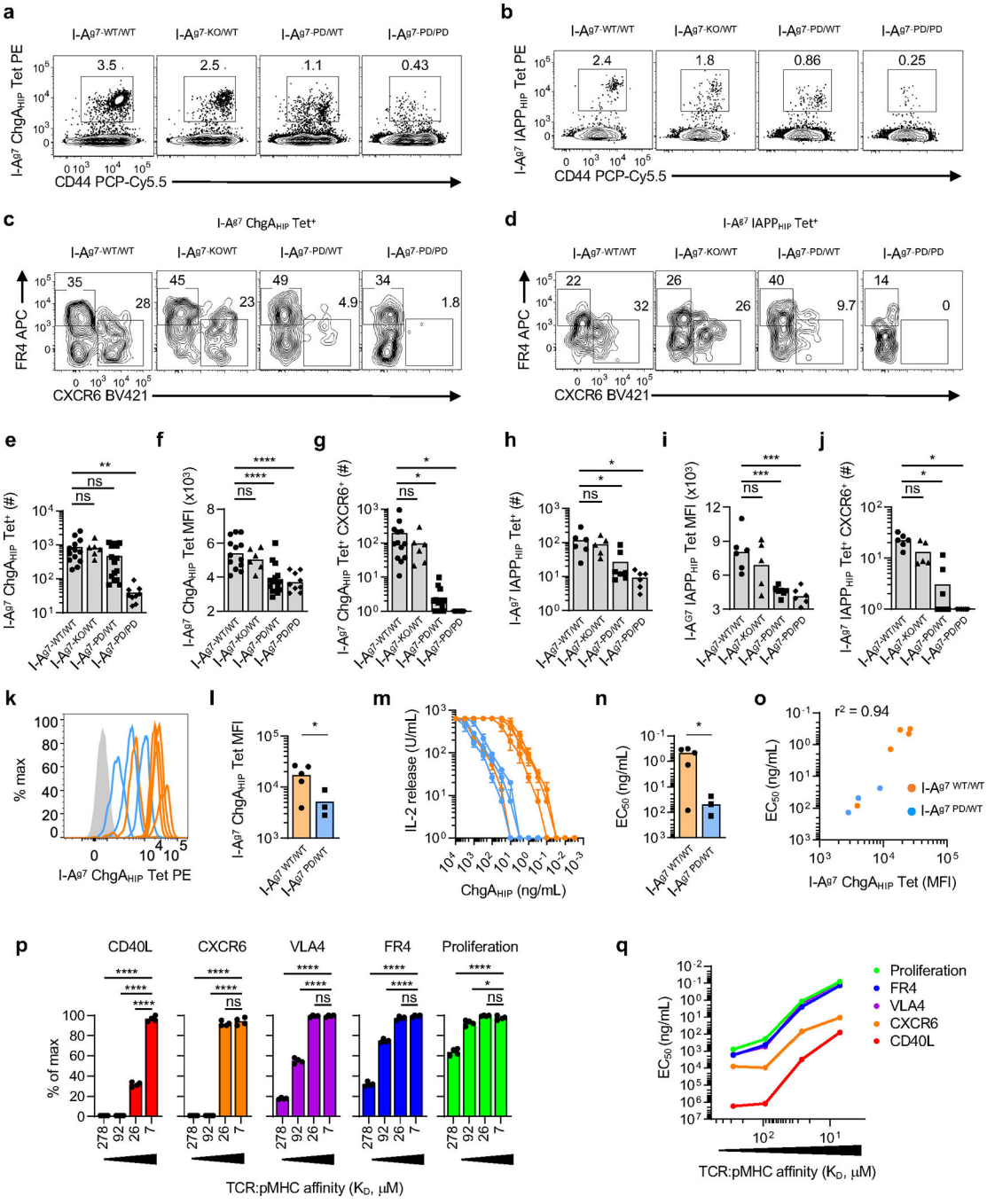

Fig. 5. Non-cognate negative selection limits of the development of β-islet specific CXCR6^{+} CD4 T cells.

(**a,b**) Flow cytometric analysis of CD4 T cells stained with (**a**) I-A^{g7}-ChgA$_{HIP}$ or (**b**) I-A^{g7}-IAPP$_{HIP}$ and CD44, following pMHC tetramer-enrichment from 12–14 weeks old non-diabetic I-A$^{g7\text{-}WT/WT}$, I-A$^{g7\text{-}KO/WT}$, I-A$^{g7\text{-}PD/WT}$ and I-A$^{g7\text{-}PD/PD}$ mice. (**c**) Expression of CXCR6 or FR4 on I-A^{g7}-ChgA$_{HIP}$ or (**d**) I-A^{g7}-IAPP$_{HIP}$ specific CD4 T cells. (**e**) Quantification of I-A^{g7}-ChgA$_{HIP}$ reactive CD4 T cells, (**f**) tetramer MFI and (**g**) CXCR6^{+} CD4 T cells from I-A$^{g7\text{-}WT/WT}$ (n=13), I-A$^{g7\text{-}KO/WT}$ (n=6), I-A$^{g7\text{-}PD/WT}$ (n=15) and

I-$A^{g7\text{-}PD/PD}$ (n=9) mice. (**h**) Quantification of I-A^{g7}-$IAPP_{HIP}$ reactive CD4 T cells, (**i**) tetramer MFI and (**j**) $CXCR6^{+}$ CD4 T cells from I-$A^{g7\text{-}WT/WT}$ (n=6), I-$A^{g7\text{-}KO/WT}$ (n=5), I-$A^{g7\text{-}PD/WT}$ (n=7) and I-$A^{g7\text{-}PD/PD}$ (n=6) mice. (**k-o**) I-A^{g7}-$ChgA_{HIP}$ tetramer staining of T cell hybridomas generated from I-$A^{g7\text{-}WT/WT}$ (orange) or I-$A^{g7\text{-}PD/WT}$ (blue) mice. (**l**) Quantification of tetramer staining MFI. (**m,n**) Activation and quantification of EC_{50} values of $ChgA_{HIP}$-reactive T cell hybridomas in response to titrating amounts of $ChgA_{HIP}$ peptide. (**o**) Correlation analyses of EC_{50} values and $ChgA_{HIP}$ tetramer staining (n=8). (**p,q**) Differential dependence on TCR:pMHC affinity and antigen concentration for CD4 T cell effector functions. Replicate wells from 2 independent experiment of B3K506 Tg T cells were activated with titrating concentrations of strong (K_D = 7μM), medium (K_D = 27μM), weak (K_D = 92μM) and very weak (K_D = 278μM) affinity ligands and expression of CD40L, CXCR6, VLA4 and FR4 was evaluated, as well as cellular proliferation. (**p**) Bar graphs indicate percent max of the effector function at 1μM peptide concentration, while (**q**) compares TCR:pMHC affinity with the EC_{50} values of effector function. ns $P>0.05$, * $P<0.05$, *** $P<0.001$, **** $P<0.0001$ (one-way ANOVA with Tukeys multiple comparisons test), r^2 Peasron's.

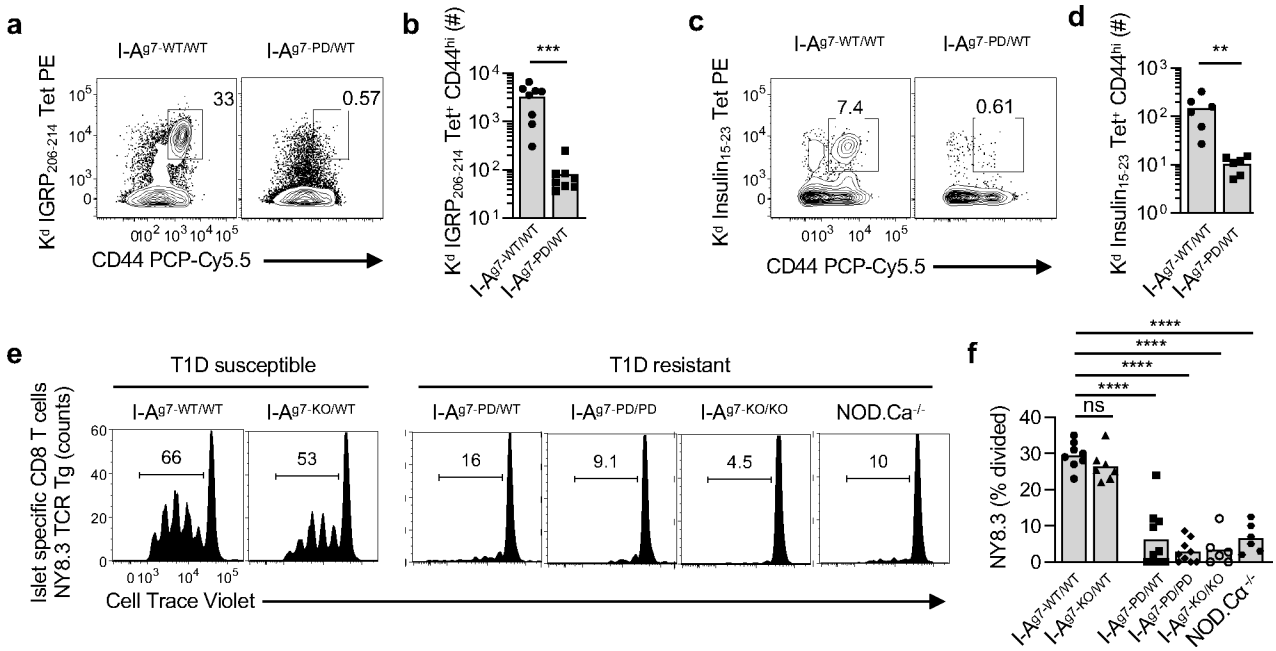

Fig. 6. I-A$^{g7\text{-}PD}$-expressing mice lack CD4 T cells capable of inducing MHC-I cross-priming of Insulin and IGRP specific CD8 T cells

(**a-d**) Flow cytometric analysis and quantification of CD8 T cells stained with (**a,b**) K^{d}-IGRP$_{206–214}$ or (**c,d**) K^{d}-Insulin$_{15–23}$ isolated from naïve I-A$^{g7\text{-}WT/WT}$ (n= 8, 6) and I-A$^{g7\text{-}PD/WT}$ (n= 8, 6) mice following pMHC tetramer-enrichment. ns P>0.05, ** P<0.01, *** P<0.001 (unpaired two-tailed t test). (**e**,**f**) Flow cytometric analysis and quantification of CTV-labelled IGRP$_{206–214}$ specific NY8.3 CD8 T cells transferred into I-A$^{g7\text{-}WT/WT}$ (n=8), I-A$^{g7\text{-}KO/WT}$ (n=7), I-A$^{g7\text{-}PD/WT}$ (n=10), I-A$^{g7\text{-}PD/PD}$ (n=9), I-A$^{g7\text{-}KO/KO}$ (n=6) or NOD.Ca$^{-/-}$ (n=6) mice. T cell proliferation was analyzed for cells isolated from the pancLN. ns P >0.05, ****P < 0.0001 (one-way ANOVA with Tukeys multiple comparisons test).

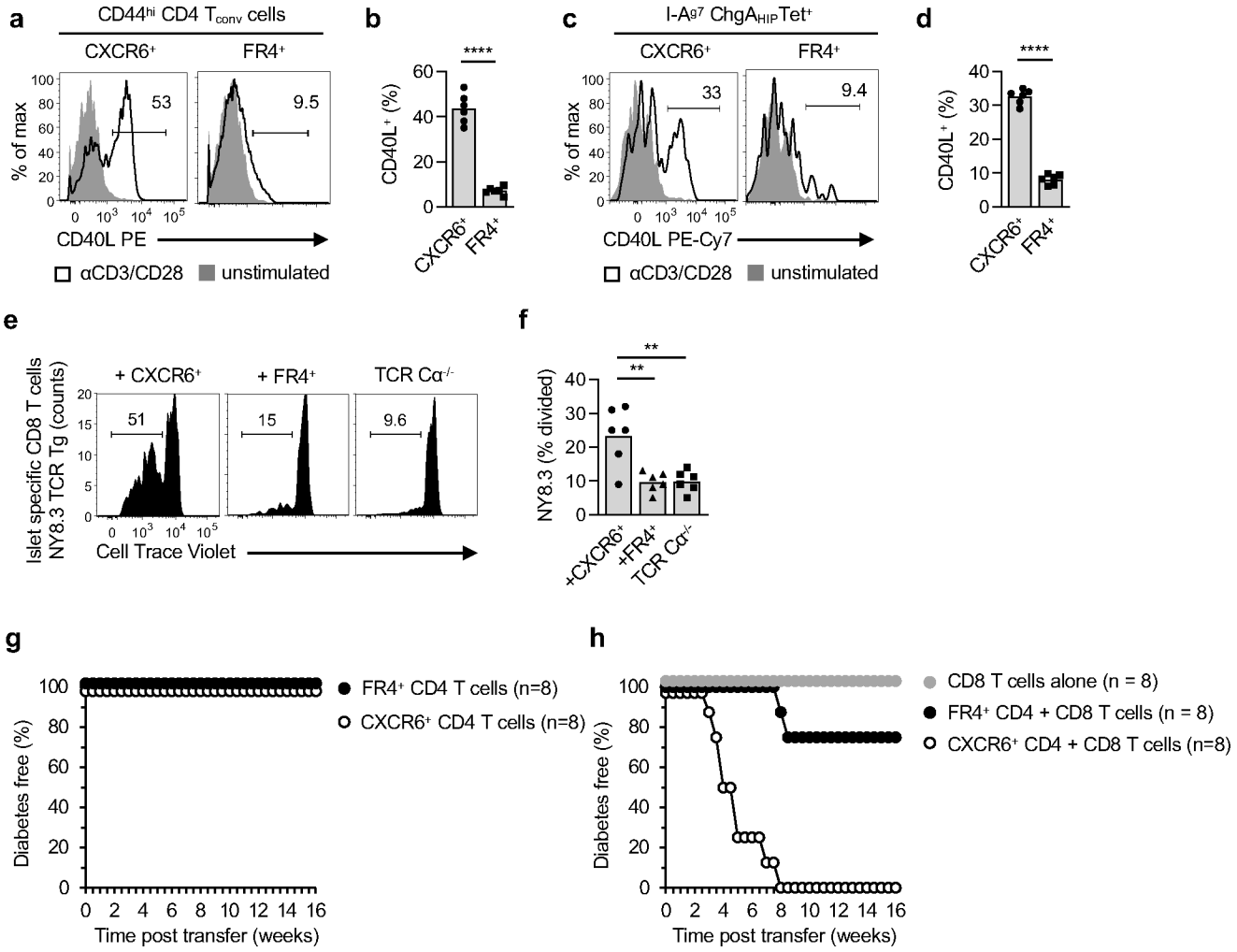

Fig. 7. CXCR6$^+$ CD4 T cells induce β-islet antigen specific CD8 T cells cross-priming of and drive T1D development

(**a, b**) Flow cytometric analysis and quantification of CD40L expression on CXCR6$^+$ and FR4$^+$ splenic (n= 6) and (**c, d**) I-A^{g7} ChgA$_{HIP}$ tetramer$^+$ (n=6) CD4 T cells following 4hrs *in vitro* stimulation with anti-CD3/CD28. **** P<0.0001 (unpaired two-tailed t test). (**e**) Representative flow cytometric analysis and (**f**) quantification of CTV-labelled NY8.3 CD8 T cells isolated from the pancLN following transferred into NOD.Ca$^{-/-}$ recipients at 8 weeks of age that previous received FACS sorted CXCR6$^+$, FR4$^+$ or no CD4 T cells from 12 weeks old NOD mice 2 weeks prior. ** P <0.01, *** P < 0.001 (one-way ANOVA with Tukeys multiple comparisons test). (**g**) T1D incidence of NOD.Ca$^{-/-}$ recipients (n=8) that received CXCR6$^+$ or FR4$^+$ CD4 T cells isolated from I-A$^{g7\text{-}WT/WT}$, or (**h**) NOD.Ca$^{-/-}$ recipients (n=8) that received CXCR6$^+$, FR4$^+$ or no CD4 T cells in addition to polyclonal CD8 T cells from I-A$^{g7\text{-}WT/WT}$ mice.